Chemie Ingenieur Technik

Resource-efficient Alkane Selective Oxidation on New Crystalline Solids: Searching for Novel Catalyst Materials

Journal:	*Chemie Ingenieur Technik*
Manuscript ID:	Draft
Wiley - Manuscript type:	Forschungsarbeit
Date Submitted by the Author:	n/a
Complete List of Authors:	Welker-Nieuwoudt, Cathrin; BASF SE, Chemicals Research and Engineering Glaum, Robert; Universität Bonn, Institut für Anorganische Chemie Dobner, Cornelia-Katharina; BASF SE, Chemicals Research and Engineering Eichelbaum, Maik; Fritz-Haber Institut der Max-Planck Gesellschaft, Abtlg. für Anorganische Chemie Gruchow, Falk; Max-Planck-Institut für Chemische Physik fester Stoffe, Heine, Christian; Fritz-Haber Institut der Max-Planck Gesellschaft, Abtlg. für Anorganische Chemie Karpov, Andrey; BASF SE, Chemicals Research and Engineering Kniep, Rüdiger; Max-Planck-Institut für Chemische Physik fester Stoffe, Rosowksi, Frank; BASF SE, Chemicals Research and Engineering Schlögl, Robert; Fritz-Haber Institut der Max-Planck Gesellschaft, Abtlg. für Anorganische Chemie Schunk, Stephan; hte AG, Titlbach, Sven; Universität Bonn, Institut für Anorganische Chemie Trunschke, Annette; Fritz-Haber Institut der Max-Planck Gesellschaft, Abtlg. für Anorganische Chemie
Keywords:	Katalyse, Oxidation, Butan, Vanadium

Ressourcen-effiziente Alkanselektivoxidation an neuen kristallinen Festkörpern: Auf der Suche nach neuartigen Katalysatormaterialien

Resource-efficient Alkane Selective Oxidation on New Crystalline Solids: Searching for Novel Catalyst Materials

Robert Glaum[2*], Cathrin Welker-Nieuwoudt[1], Cornelia-Katharina Dobner[1], Maik Eichelbaum[4], Falk Gruchow[5], Christian Heine[4], Andrey Karpov[1], Rüdiger Kniep[5], Frank Rosowski[1], Robert Schlögl[4], Stephan Andreas Schunk[3], Sven Titlbach[2] and Annette Trunschke[4]

[1] BASF SE, Chemicals Research and Engineering, Carl-Bosch-Straße 38, D-67056 Ludwigshafen, Germany
[2] Institut für Anorganische Chemie, Universität Bonn, Gerhard-Domagk-Str. 1, D-53121 Bonn, Germany
[3] hte AG, Kurpfalzring 104, D-69123, Heidelberg, Germany.
[4] Fritz-Haber-Institut der Max-Planck-Gesellschaft, Abtlg. für Anorganische Chemie, Faradayweg 4-6, D-14195 Berlin, Germany.
[5] Max-Planck-Institut für Chemische Physik fester Stoffe, Nöthnitzer Straße 40, D-01187 Dresden, Germany.

Abstract

A total of 29 hitherto unknown vanadyl(IV)-, vanadyl(V)-, and vanadate(V)-phosphates were synthesized, structurally characterized, and tested in terms of their behaviour as catalysts in the selective oxidation of *n*-butane to maleic anhydride (MA). The series of compounds comprises silver-vanadyl-phosphates, vanadium-borophosphates, the vanadyl(V)-phosphates $Fe(V^{V}O)(PO_4)_2$ and $(V^{V}O)Ti_6(PO_4)_9$, vanadium(V)-substituted pyrophosphates $Fe_4[(P_{1-x}V_x)_2O_7]_3$ and $Ti(P_{1-x}V_x)_2O_7$, as well as some zirconium- and

niobium-phosphates with phosphorus partially substituted by vanadium. The new materials did not surpass the performance of commercially used $(V^{IV}O)_2P_2O_7$ based catalysts, but a silver-vanadium-phosphate of approximate composition $Ag_2V^{IV,V}P_{1.6}O_{7+\delta}$ ($0 \leq \delta \leq 0.5$), supposedly having a vanadyl(IV, V) phosphate pyrophosphate layer structure, shows promising activity and selectivity ($X_{n\text{-butane}}$ = 24%, S_{MA} = 13%) with potential for further improvements. With the aim to study the charge carrier dynamics of the synthesized catalysts under the conditions of the target redox reaction, we have developed a new method for *in situ* non-contact measurement of the electric conductivity of catalysts. The analysis of conductivity changes in response to the chemical potential of oxygen in the gas phase offers valuable clues to understand structure-reactivity relationships in selective oxidation catalysis.

Zusammenfassung

Neunundzwanzig bislang nahezu vollständig unbekannte Vanadyl(IV)-, Vanadyl(V)- und Vanadat(V)-phosphate wurden dargestellt, bezüglich ihrer Kristallstruktur charakterisiert und im Hinblick auf ihre Eignung als Katalysatormaterialien für die Selektivoxidation von *n*-Butan untersucht. Die Reihe an Verbindungen umfaßt Silber-vanadyl-phosphate, Vanadium-borophosphate, die Vanadyl(V)-phosphate $Fe(V^{V}O)(PO_4)_2$ und $(V^{V}O)Ti_6(PO_4)_9$, mit Vanadium(V) substituierte Pyrophosphate $Fe_4[(P_{1-x}V_x)_2O_7]_3$ und $Ti(P_{1-x}V_x)_2O_7$, sowie einige Phosphate von Zirkonium und Niob, bei denen ebenfalls ein Teil des Phosphors durch Vanadium isomorph ersetzt wurde. Die untersuchten Substanzen reichen in ihrer katalytischen Leistung in der Selektivoxidation von *n*-Butan zu Maleinsäureanhydrid noch nicht an das etablierte Katalysatormaterial $(V^{IV}O)_2P_2O_7$ heran. Allerdings wurde ein neues Silber-vanadyl-phosphat mit der ungefähren Zusammensetzung $Ag_2V^{IV,V}P_{1.6}O_{7+\delta}$ ($0 \leq \delta \leq 0.5$) gefunden, das nach ersten katalytischen Tests vielversprechende Umsätze und Selektivitäten ($U_{n\text{-Butan}}$ = 24%, S_{MA} = 13%) zeigt und Potential für eine Optimierung bietet. Für die Substanz wird eine Struktur mit Vanadyl(IV, V)-orthophosphat-pyrophosphat-Schichten und zwischen den Schichten befindlichen Ag^+-Ionen angenommen. Mit dem Ziel die Dynamik des Ladungsträgertransfers unter Bedingungen der Oxidationskatalyse zu studieren, wurde eine neue Methode zur kontaktlosen *in situ* Messung der elektrischen Leitfähigkeit von Katalysatoren entwickelt. Die Analyse der Leitfähigkeitsänderungen in Abhängigkeit vom chemischen Potential des Sauerstoffs in der Gasphase erlaubt wertvolle Schlüsse in Bezug auf die Identifizierung von Struktur-Reaktivitätsbeziehungen in der Oxidationskatalyse.

Keywords: Catalysis, Selective Oxidation, Solid Phases, Vanadium, Phosphate

1 Introduction

The collaborative research project ReAlSelOx ("**R**esource-**e**fficient **Al**kane **Sel**ective **Ox**idation") was part of the German Federal Ministry of Education and Research (BMBF) funding program “Innovative Technologies for Resource Efficiency – Resource-Intensive Production Processes” (r^2 funding priority). The aim of this project was to explore new classes of heterogeneous catalysts, which have the potential to yield more selective and therefore more resource-efficient materials compared to the current state-of-the-art catalysts that are the result of more than 40 years of development and optimization.

Selective oxidation of *n*-butane to maleic anhydride is one of a few successful examples of a commercialized process for the gas phase oxidation of alkanes [1]. This production process currently utilizes $(VO)_2P_2O_7$ based catalysts. Apparently, it is the unique property of this material that allows a series of cascade reactions: the abstraction of eight hydrogen atoms and the insertion of three oxygen atoms into the starting material *n*-butane, accompanied by the transfer of 14 electrons, at satisfactory maleic anhydride yields.

First reports on the use of vanadium phosphorus oxide (VPO) catalysts for the selective oxidation of butane can be traced back to 1966 when BERGMAN and FRISCH reported maleic anhydride yields of up to 31 mol.-% at reaction temperatures of 550°C [2]. Optimization of the catalyst composition and synthesis in combination with advances in process engineering allowed further improvement of maleic anhydride (MA) yields to 55 – 60 mol.-% [3]. Consequently, first commercial plants for maleic anhydride production, based on *n*-butane feedstock, were started up in the 1970s [4]. Currently, gas phase oxidation of *n*-butane has become the dominant technology for maleic anhydride production. Despite significant efforts during the last decades to improve this industrial process, the maleic anhydride yields are remaining at relatively low levels of < 65 mol.-% [5].

GRASSELLI discussed the influence of chemical composition and bulk structural properties on the catalytic behaviour of various oxide-materials in ammoxidation and oxidation of alkanes. In 1999 he suggested that further improvements of $(VO)_2P_2O_7$ based catalysts would be challenging due to their crystal-chemical peculiarities and that the search for novel catalytic lead structures would be more promising in order to achieve better yields in *n*-butane oxidation [6]. Rational approaches for alternative materials were based on the structural incorporation of vanadium(IV) in combination with other elements (*e.g.* Nb, Sb [7] or Cr, Fe, Co, Ni, Cu [8,9]) into a phosphate framework in order to achieve improved site isolation [10,11] on the catalyst surface by modification of the bulk crystal

structure. In addition, the presence of $(V=O)^{2+}$, $(V=O)^{3+}$, or $(O=V=O)^{+}$ groups and a certain nucleophilic (basic) behaviour of oxygen in the material were considered as chemical prerequisites for active and selective catalysts [12,13,14]. Recently, a search based on the aforementioned ideas led to several promising candidate materials for selective oxidation catalysts [7,8,9,15], however, without providing a real breakthrough. Despite these negative results some deeper mechanistic insights into selective oxidation were achieved in recent years [16,17]. Thus, formulation of several requirements concerning the chemical and crystal-chemical properties of a promising catalyst material has become possible, including chemical composition, nucleophilicity of surface oxygen, LUX-FLOOD acidity/basicity of the solid, and bulk structural properties.

Chemical composition. Only a limited number of transition metals with specific oxidation states show redox properties that qualify them as crucial components of catalyst materials for selective oxidation, *e.g.* vanadium(IV, V), molybdenum(V, VI), tungsten(VI), manganese(III, IV), rhenium(IV, V, VI, VII), iron(III), copper(I, II), and silver(I). The oxidation strength of the corresponding oxides is modified by formation of compounds according to general chemical rules. Thus, in agreement with the LUX-FLOOD acid-base theory (with O^{2-} as reference) [18,19], transition metals in high oxidation states are stabilized by reaction with strong basic oxides (strong oxide donors). In contrast, reaction with acidic oxides leads to destabilization (in a thermodynamic sense) of the high oxidation state. Furthermore, mixed-valence vanadium(IV, V) compounds appear to be particularly interesting, since TRIFIRO *et al.* [20] showed a correlation between the selectivity to maleic anhydride with the degree of the surface oxidation state of vanadium. ZAZHIGALOV *et al.* [21] observed optimum catalytic properties for *n*-butane oxidation on V/P-mica compounds $R_x[(V^{IV}O)_x(V^{V}O)_{1-x}PO_4]\cdot nH_2O$ at the oxidation state of vanadium ranging from 4.1 to 4.2.

Nucleophilicity of surface oxygen; Acidity/basicity of the solid. In addition to the thermodynamic stabilization/destabilization of transition metal oxides (acid/base reaction), the nucleophilicity of the (surface) oxygen atoms is modified by formation of compounds. This modification should have a direct influence on the ability of these oxygen atoms to activate C-H bonds [22].

Structural and electronic requirements. A profound understanding of charge transfer phenomena at the interface of the solid catalyst, its surface and the gas phase is a prerequisite for the rational design of materials for selective oxidation reactions. How the charge carriers and the required oxygen atoms are provided, and how the reaction proceeds on a molecular level, are still unsolved, but very pressing questions. One essential structural element of successful oxidation catalysts seems to be the

$(M{=}O)^{n+}$ unit (M = V, Mo, W, Re) [22,23]. Furthermore, simple re-arrangement mechanisms for the compensation of the loss of (surface) oxygen atoms are apparently required. The trans-vertex sharing as it is found for $[VO_6]$ octahedra in $(VO)_2P_2O_7$ and α-$VOPO_4$ allows for instance the relaxation after removal of one oxygen atom. These crystal structures show alternating short and long distances d(V-O) which easily might switch their orientation. In addition, sufficient high mobility of oxygen in the solid should be advantageous. Thus, the catalyst bulk should be able to act as “oxygen buffer” for the surface processes leading to the crystal chemical demand for a low, however, non-zero degree of connectivity of the redox-active $[MO_n]$ polyhedra. It is generally discussed and supporting arguments are provided, *e.g.* based on oxygen isotopic labeling [24,25], temporal analysis of products [26], *in situ* microbalance [27] and transient kinetic investigations [28], that oxygen from an active site on the surface of the catalyst is abstracted in order to activate and oxidize the alkane, whereas the catalyst is subsequently re-oxidized by gas phase O_2 in the stationary state. Eventually, the concentration of the redox-active atoms at the surface should not be too high to minimize the total oxidation of the substrate (“site isolation concept“ [10]). However, it is also controversially debated if single non-interacting active sites on the surface consisting of only a limited number of redox active transition metal ions are involved, while the bulk catalyst plays only the role of an inert support. Alternatively, bulk charge carriers (electrons, holes, oxygen ions) might be involved in the reaction as well. The single-site concept would require rather large active sites to provide the necessary charge carriers in a single reaction path. In contrast, the unlimited availability of bulk oxygen and charge carriers would be in conflict with the fundamental site-isolation principle [29] of selective oxidation catalysts requiring the (ideally stoichiometric) limitation and spatial separation of active oxygen and transition metal species in order to avoid the total oxidation of the desired product.

The present work is based on the principles of rational catalyst design. An integrated methodology encompassing new synthetic approaches combined with accelerated catalytic screening and *in situ* experimental studies of the state of the catalysts under reaction mechanisms was applied. Based on the knowledge outlined above, the following two synthetic concepts have been pursued:

1) Search for further polynary vanadyl(IV)-phosphates in addition to the well-known $M^{II}V_2O_2(PO_4)_2$ (M^{II}: Fe, Co, Ni, Cu) and $M^{III}V_3O_3(PO_4)_3$ (M^{III}: V, Cr, Fe).

2) Search for hitherto unknown polynary vanadyl(V)-phosphates and/or phosphate-vanadates(V). The latter area is in particular suggested by the idea of "taming" the too strongly (and unselectively) oxidizing V_2O_5 in such compounds.

In detail, the following compounds have been studied for their use as catalyst materials in the selective oxidation of *n*-butane: 1) silver-vanadyl(IV, V)-phosphates, 2) vanadium-borophosphates and borate-phosphates, 3) compounds in the ternary systems $FeO_{1.5}$ / $VO_{2.5}$ / $PO_{2.5}$, 4) TiO_2 / $VO_{2.5}$ / $PO_{2.5}$, 5) ZrO_2 / $VO_{2.5}$ / $PO_{2.5}$, and 6) $NbO_{2.5}$ / $VO_{2.5}$ / $PO_{2.5}$. Since the transfer of charge carriers on the surface as well as in the bulk is considered to be crucial for an efficient oxidation catalyst, our project also included the development of a novel method to determine *in situ* those properties.

The impact of structural and electronic features, in particular of the $[V_xO_y]$ substructures in the new phosphates on their catalytic behaviour will be discussed and compared to $(VO)_2P_2O_7$ and its structural and electronic properties.

2 Experimental

2.1 Catalyst Preparation

Vanadyl(IV)-pyrophosphate. The investigated $(VO)_2P_2O_7$ reference catalyst was synthesized and characterized as recently described in [30].

Silver-vanadyl-phosphates. A series of different solid phases of general composition $Ag_2VP_xO_d$ ($1 \le x \le 2$; $6 \le d \le 8$) were prepared using wet chemistry methods [31]. One of these compounds, *viz.* $\mathbf{Ag_2V^{IV,V}P_{1.6}O_{7+\delta}}$ ($0 \le \delta \le 0.5$; Cat-1), was unknown in literature. These syntheses consisted of the reaction of a silver source ($AgNO_3$ or Ag_2O) with V_2O_5 and a phosphorus source such as H_3PO_4 and/or H_3PO_3 in water under reflux with continuous stirring. The resulting suspensions were either spray-dried or the solid in the suspension was recovered by filtration, washed with water and dried under vacuum at 90 °C. Its XRPD pattern [31] shows some similarity to those of $Ag_{0.43}V^{IV,V}O(PO_4)$ [32], $Ag_2(V^VO_2)(PO_4)$ [33] and $Ag_6(V^{IV}O)_2(PO_4)_2(P_2O_7)$ [34]. The latter has only recently been structurally characterized as a mixed orthophosphate-pyrophosphate (*cf.* section 3, Figure 2).

In addition $\mathbf{Ag(V^{IV}O)(V^VO)(PO_4)_2}$ (Cat-2) [35] was tested. It was synthesized from literature by reacting $AgNO_3$, V_2O_5, and $(NH_4)_2HPO_4$ in the molar ratio 1 : 0.9 : 2 for 24 h at 380 °C in air. After complete evaporation of all volatile species vanadium was added as reductant to set the desired composition. After reaction at 550 °C (72 h) in a sealed silica tube, silver-vanadyl(IV)-vanadyl(V)-orthophosphate was obtained as brown, microcrystalline single-phase powder.

Vanadium-containing borophosphates and borate-phosphates. As yet, no template-free vanadium(IV, V)-borophosphates are known. A detailed investigation of the

systems $VO_{2/2.5}$ / $BO_{1.5}$ / $PO_{2.5}$ under equilibrium conditions did not lead to new compounds and no solid solutions were found. Since most borophosphates [36] and the precursor phase for $(VO)_2P_2O_7$, $VOHPO_4 \cdot 1/2\,H_2O$, are synthesized under hydrothermal conditions [37], our study included the systems $VO_{2/2.5}$ / $BO_{1.5}$ / $PO_{2.5}$ / H_2O. Thus, the new compound **$(V^{IV}O)_2[B(OH)_4][PO_4]$** (Cat-3) was synthesized and characterized [38]. Its structure was eludicated using X-ray single-crystal data (*cf.* section 3, Figure 3). Samples of $(V^{IV}O)_2[B(OH)_4][PO_4]$ for catalytic testing were synthesized hydrothermally. For this purpose a mixture of VO_2, BPO_4 and water (total weight 26 g, molar ratio 1 : 2 : 77) was filled into a teflon autoclave (V = 50 mL; filling degree 50%) and heated at 170 °C for five days. The product was separated from the mother liquor by vacuum filtration, washed with water and dried at 60 °C. Thermogravimetric studies of $(V^{IV}O)_2[B(OH)_4][PO_4]$ in argon show a loss of two equivalents of water, in agreement with the formula.

The only known anhydrous compound in the system $VO_{1.5}$ / $BO_{1.5}$ / $PO_{2.5}$ / (H_2O) is $V^{III}{}_2[BP_3O_{12}]$ [39]. An extension of the study to the systems $VO_{1.5}$ / $BO_{1.5}$ / $PO_{2.5}$ / H_2O led to the discovery of the new borophosphate $V^{III}[B_2P_2O_7(OH)_5]$, which is isotypic to $Fe^{III}[B_2P_2O_7(OH)_5]$ according to its XRPD pattern [40]. Its crystal structure (*cf.* section 3, Figure 4) was refined from XRPD data using the Rietveld method [38]. For catalytic testing three compounds were chosen and tested under different reaction conditions. For the synthesis of **$V^{III}[B_2P_2O_7(OH)_5]$** (Cat-4) a mixture of V_2O_3, H_3BO_3, H_3PO_4 85%, and a 10 wt% HCl solution (total weight 12 g, molar ratio 1 : 4 : 4 : 30) was loaded into a teflon autoclave (V = 25 mL; filling degree 40%) and heated to and maintained at 170 °C for five days. The product was separated from the mother liquor by vacuum filtration, washed with water and ethanol and dried at 60 °C. Chemical analysis of the final product confirms the absence of chlorine and the elemental composition $V^{III}[B_2P_2O_7(OH)_5]$.

For synthesis of **$Fe_{0.5}V_{0.5}[B_2P_2O_7(OH)_5]$** (Cat-5) a mixture of Fe_2O_3, V_2O_3, H_3BO_3, H_3PO_4 85% and a 15 wt% HCl solution (total weight 12 g, molar ratio 1 : 1 : 2 : 2 : 15) was filled into a teflon autoclave (V = 25 mL; filling degree 40%) and heated at 170 °C for five days. The product was separated from the mother liquor by vacuum filtration, washed with water and ethanol and dried at 60 °C.

While vanadium(III) is usually inactive in selective oxidation reactions, it was the aim to obtain active catalysts either by partial substitution of V^{3+} by Fe^{3+} or by oxidation of V^{3+} under reaction conditions.

The known phase **$V^{III}{}_2[BP_3O_{12}]$** (Cat-6) was differently synthesized than described in [39]. A mixture of H_3PO_4, H_3BO_3 and V_2O_5 was heated to and maintained at 90 °C and

stirred for 16 hrs. The solution was then spray-dried and calcined at 480 °C in air for 20 hrs.

$FeO_{1.5}$ / $VO_{2.5}$ / $PO_{2.5}$: In this system the new phosphate **$Fe(V^{V}O)(PO_4)_2$** (tetragonal, a = 8.6313(6) Å, c = 9.0211(5) Å; structurally related to $(V^{IV}O)Si(PO_4)_2$ [41,42]), as well as the three solid solutions **$Fe^{III}_4[(P_{1-x}V_x)_2O_7]_3$** ($0 \le x \le 0.75$), $Fe(V_{1-x}P_x)O_4$ ($0 \le x \le 0.5$), and $Fe_2(V_{1-x}P_x)_4O_{12}$ ($0 \le x \le 0.4$) were identified as equilibrium phases [43].

For the syntheses of about 2 g of catalyst material, intensely red coloured aqueous suspensions of $Fe(acac)_3$ were mixed with appropriate amounts of $VO(acac)_2$ and $(NH_4)_2HPO_4$ in diluted nitric acid. While stirring, these mixtures were dried in a beaker on a hot-plate at ϑ_{max} = 150 °C. For removal of nitrous gases and completion of the reactions the obtained residues were subsequently heated in silica crucibles at 400 °C in air for 48 h. The resulting residues were amorphous according to XRPD (IP-Guinier photographs). To produce crystalline materials, a third heating period at 700 °C followed. Six samples were chosen for catalytic testing (*cf.* Table 1): "$Fe^{III}(V^{V}O)(PO_4)_2$" (400 °C, amorphous; Cat-7), $Fe^{III}(V^{V}O)(PO_4)_2$ (700 °C, crystalline; Cat-8), "$Fe^{III}_4[(P_{0.83}V_{0.16})_2O_7]_3$" (400 °C, amorphous; Cat-9), $Fe^{III}_4[(P_{0.83}V_{0.16})_2O_7]_3$ (700 °C, crystalline, $V_4(P_2O_7)_3$ structure type [44], a = 21.635(7), b = 7.380(1), c = 9.577(7) Å; Cat-10), "$Fe^{III}_4[(P_{0.25}V_{0.75})_2O_7]_3$" (400 °C, amorphous; Cat-11), $Fe^{III}_4[(P_{0.25}V_{0.75})_2O_7]_3$ (700 °C, crystalline, $V_4(P_2O_7)_3$ structure type [44], a = 22.923(9), b = 7.546(2), c = 9.954(6) Å; Cat-12).

System TiO_2 / $VO_{2.5}$ / $PO_{2.5}$: During detailed equilibrium investigations [45] the new compound **$(V^{V}O)Ti^{IV}_6(PO_4)_9$** was observed and its crystal structure determined [45,46]. In addition, the solid solution **$Ti(P_{1-x}V_x)_2O_7$** (phosphorus-rich: $0 \le x \le 0.24$; vanadium-rich: $0.30 \le x \le 0.43$) was obtained. Interestingly, the miscibility gap is caused by the equilibrium between $(V^{V}O)Ti^{IV}_6(PO_4)_9$ and V_2O_5.

For the synthesis of the catalyst materials the same procedures were applied as described for the iron-containing compounds. As starting materials meta titanic acid or titanyl(IV)-acetylacetonate-hydrate were used. Prior to their use, the titania content of these precursors was gravimetrically determined. Intermediate heating was performed at 450 °C and the final calcination step at 700 °C.

Six samples were tested for their catalytic behaviour (*cf.* Table 1): "$(V^{V}O)Ti^{IV}_6(PO_4)_9$" (450 °C, amorphous; Cat-13), $(V^{V}O)Ti^{IV}_6(PO_4)_9$ (700 °C, crystalline; Cat-14), $Ti(P_{0.8}V_{0.2})_2O_7$ (P-rich; 450 °C, amorphous; Cat-15), $Ti(P_{0.8}V_{0.2})_2O_7$ (P-rich; 700 °C, crystalline; Cat-16), $Ti(P_{0.6}V_{0.4})_2O_7$ (V-rich; 450 °C, amorphous; Cat-17), and $Ti(P_{0.6}V_{0.4})_2O_7$ (V-rich; 700 °C, crystalline; Cat-18).

System ZrO_2 / $VO_{2.5}$ / $PO_{2.5}$. At temperatures of around 700 °C formation of the solid solution $\mathbf{Zr(P_{1-x}V_x)_2O_7}$ ($0 \le x \le 1$) is observed [47]. Above the thermal stability limit of the solid solution, at 1080 °C, the equilibrium phases $Zr_2O(PO_4)_2$(s) [48], ZrO_2(s), and $VO_{2.5}$(l) are formed over a wide compositional range. A limited substitution of phosphorus by vanadium in the oxide-phosphate (according to $\mathbf{Zr_2O(P_{0.95}V_{0.05}O_4)}$) is indicated by a small shift of the reflections in the XRPD and by ^{51}V-MAS-NMR [45]. Six microcrystalline samples were catalytically tested (*cf.* Table 1): ZrV_2O_7 (450 °C and 450 °C followed by 700 °C; Cat-19 and Cat-20, respectively), $Zr(V_{0.5}P_{0.5})_2O_7$ (450 °C and 450 °C followed by 700 °C; Cat-21 and Cat-22, respectively), and $Zr_2O[(P_{0.95}V_{0.05})O_4]_2$ (450 °C and 450 °C followed by 1080 °C; Cat-23 and Cat-24, respectively). As starting materials zirconyl-acetylacetonate-hydrate, NH_4VO_3 and H_3PO_4 were used.

System $NbO_{2.5}$ / $VO_{2.5}$ / $PO_{2.5}$. For catalytic testing $\mathbf{VNb(PO_4)_3}$, which has already been reported in literature [49], as well as the 3 x 3 block structures $\mathbf{VNb_9O_{25}}$ [50] and $\mathbf{V_{0.5}P_{0.5}Nb_9O_{25}}$ were synthesized. For the system VNb_9O_{25} / PNb_9O_{25} complete miscibility was observed [45]. For synthesis, stoichiometric amounts of $Nb(HC_2O_4)_5$ or $NH_4NbO(C_2O_4)_2$ as niobia source, NH_4VO_3, and $(NH_4)_2HPO_4$ were dissolved in oxalic acid (0.5 mol/l), resulting in blue solutions. After drying these solutions via evaporation on a hot plate, followed by heating for 10 h at 450°C in air, light-blue greenish powders were obtained.

Optionally, the products were exposed to a second heating cycle for 3 d between 700 °C to 1000 °C at reduced oxygen pressure ($p(O_2) \approx 10^{-6}$ bar). The following materials were tested for their catalytic behaviour: "$V^VNb_9O_{25}$" (450 °C; according to XRPD *T*-Nb_2O_5 [51]; Cat-25), $V^VNb_9O_{25}$ (450 °C followed by 1000 °C; Cat-26), "$(V^V_{0.5}P_{0.5})Nb_9O_{25}$" (450 °C; according to XRPD *T*-Nb_2O_5 [51]; Cat-27), "$(V^V_{0.5}P_{0.5})Nb_9O_{25}$ (450 °C followed by 1000 °C; Cat-28), and amorphous "$VNb(PO_4)_3$" (450 °C; Cat-29). Interestingly, phases with the XRPD pattern of *T*-Nb_2O_5 have never been obtained in reference experiments without vanadium. This is an indication for the incorporation of vanadium into this structure according to the formulation *T*-$(Nb_{1-x}V_x)_2O_5$ (*cf.* Section 3).

2.2 Characterization

The atomic element ratios for the Ag-V-P-O and V-B-P-O catalyst precursors were analyzed by atomic emission spectrometry with inductively coupled plasma (Varian Vista Pro or Varian Vista RL).

Micro-crystalline phases present in the catalyst precursors and used catalysts were determined by X-ray powder diffraction. For this purpose a D 8 Advance Series 2, Bruker-AXS diffractometer equipped with an energy dispersive Sol-X detector, operating

at 40 kV and 40 mA (Cu-K_α radiation, λ = 0.154 nm) was used. Alternatively, *IP*-Guinier photographs were used for XRPD studies (camera Huber G670 or camera FR-552 Enraf-Nonius, Cu-$K\alpha_1$ radiation, quartz monochromator, image plate technique [52,53]). Details on this technique have already been reported in [54].

The NMR experiments were carried out on a Varian Infinity+ spectrometer equipped with a commercial 2.5 mm MAS NMR double-resonance probe. The magnetic field strength was 9.4 T corresponding to a ^{31}P and ^{51}V resonance frequency of 162.61 and 105.53 MHz, respectively. The ^{31}P chemical shifts refer to an 85% aqueous solution of H_3PO_4, the ^{51}V chemical shifts to $VOCl_3$.

2.3 *In situ* non-contact conductivity measurement of catalysts

Conventional contact methods for measuring electrical conductivity and hence charge transfer properties of catalysts under working conditions are hampered by contact resistances between electrodes and catalyst particles making very sensitive and accurate *in situ* measurements challenging. We developed a method based on the microwave cavity perturbation technique (MCPT) [55], perfectly suited to study the electrical conductivity of catalysts under true reaction conditions in a non-contact and non-invasive manner (Figure 1, [56]). The technique relies on the adiabatic change of the characteristics (resonance frequency, quality factor) of a microwave resonator (cavity) upon the introduction of the sample under investigation. This enables the direct determination of the complex permittivity and electrical conductivity of the sample. In contrast to conventional DC and low-frequency AC 2-contact methods, which essentially measure intergrain, interparticle and electrode-particle contacts, non-contact MCPT probes grain (materials) properties. This represents a substantial advantage in view of the investigation of heterogeneously catalyzed reactions at an atomic or molecular level. The developed instrument consists of a quartz tube fixed-bed flow-through reactor inserted into an X-band TM110 microwave cavity (ZWG Berlin-Adlershof) operating at 9.2 GHz generated by a network analyzer (Agilent PNA-L calibrated with the electronic calibration module Agilent N4691B ECal) (Figure 1). The reactor tube is connected to an external furnace for preheating a gas stream to provide the desired temperatures at the sample, to a gas delivery manifold for inert and reaction gases, and to an on line GC gas analysis system (Agilent 7890A) allowing the simultaneous measurement of the catalytic performance. The apparatus was calibrated with various single-crystals and powders with known complex permittivity in order to measure absolute permittivity and conductivity values [56]. The method was successfully tested for studying the temperature dependence of the complex permittivity and electrical conductivity of a VPO

catalyst in the selective oxidation of *n*-butane to maleic anhydride under industrially relevant reaction conditions [30].

2.4 Catalyst Testing

All catalyst samples were tested in a 48-fold test reactor at a sample volume of 1 ml at a particle size fraction of 500 to 1000 µm. The type of testing equipment used for this study can be considered “Stage II”, meaning that it allows differentiation of catalyst performance on a detailed level. The temperature variations in the apparatus are on the scale of ±1 °C and carbon balances can in general be closed up to a level of ±2% [57]. The different materials were first exposed to a sequence of conditioning steps involving a slow and steady rise in temperature as well as in the *n*-butane content to the desired levels. The standard testing conditions involved temperature changes with a gas feed of 2% *n*-butane in air at a GHSV of 2000 h^{-1}, typical temperature levels ranged between 380 and 420 °C. Typically, during the testing sequence, the conditions were repeated to see whether catalyst samples have suffered under the given conditions. The data were evaluated automatically using the commercial software tool “myhte” [58].

In order to check reproducibility the following strategy was pursued: within a given set of catalyst candidates, which were tested in the test unit, a number of standard catalysts (typically 3-5) were randomly distributed. These standard catalysts were used as internal reference to determine deviations within one run as well as for comparison of different runs.

3 Results and discussion

3.1 Crystal Structures

The catalysts under investigation show varied chemical compositions and structural features. The characteristics of the involved crystal structures are summarized below.

Silver-vanadium-phosphates. A number of phosphates have been tested in this system [31]. In the meantime the best catalyst in this series, described in [31] by the empirical formula $Ag_2V^{IV,V}P_{1.6}O_{7+\delta}$, was characterized structurally [59]. In agreement with this new investigation, the compound has to be regarded as mixed orthophosphate-pyrophosphate $Ag_6(V^{IV}O)_2(PO_4)_2(P_2O_7)$. It consists of anionic layers $[(V^{IV}O)_2(PO_4)_2(P_2O_7)]^{6-}$ with Ag^+ ions in-between (Figure 2b; [59]). Interestingly, there is some similarity to the layers $[(V^{V}O_2)(PO_4)]^{2-}$ reported for $Ag_2(V^{V}O_2)(PO_4)$ (Figure 2a; [33]). In addition, the hitherto unknown catalytic behaviour of $Ag(V^{IV}O)(V^{V}O)(PO_4)_2$ [35]

has been characterized. This mixed vanadyl(IV, V)-orthophosphate was studied since it shows all the structural features which are deemed necessary for a promising selective oxidation catalyst (mixed valent vanadium(IV, V), vanadyl-groups, linkage of $[VO_6]$ octahedra, *cf.* [35]; Figure 2c).

Vanadium borophosphates. The crystal structure of the new vanadium borate-phosphate $(V^{IV}O)_2[B(OH)_4][PO_4]$ (*P4/ncc* (no.130), *a* = 6.2763(2) Å, *c* = 8.1572(2) Å, *Z* = 4, Figure 3a and b; [38]) comprises $[(V^{IV}{=}O)O_5]$ octahedra and statistically distributed $[B(OH)_4]^-$ and $[PO_4]^{3-}$ tetrahedra. In agreement with valence sum considerations and based on comparison to similar compounds already reported in literature (*e.g.* mineral seamanite $Mn_3[B(OH)_4][PO_4](OH)_2$ [60]), we assume that the protons are exclusively attached to the V-O_b-B bridging oxygen atoms. Thus, evidence is given to the formulation of $[B(OH)_4]^-$ anions. The structure of $(V^{IV}O)_2[B(OH)_4][PO_4]$ is closely related to that of α_I-$V^{V}OPO_4$ [61] (Figure 3c and d) with a doubled *c*-axis. In both structures the $[VO_6]$ octahedra are connected to chains with alternating short and long distances *d*(V-O) [62].

The crystal structure of the new vanadium borophosphate $V^{III}[B_2P_2O_7(OH)_5]$ (*C2/c* (no. 15), *a* = 17.7121(8) Å, *b* = 6.7483(2) Å, *c* = 7.0389(2) A, β = 108.737(2)°, *Z* = 4; Figure 4) comprises of isolated $V^{III}O_6$ octahedra and alternatingly connected $PO_3(OH)$ and $BO_2(OH)(OH_{0.5})$ tetrahedra. The tetahedra are alternatingly connected via common vertices forming 1D infinite $[B_2P_2O_7(OH)_5]^{3-}$ polyanions, which show some resemblance to *catena*-metaphosphate anions PO_3^-.

Iron-vanadium(V)-phosphates. In the system $FeO_{1.5}$ / $VO_{2.5}$ / $PO_{2.5}$ the hitherto unknown iron(III)-vanadyl(V)-orthophosphate $Fe(V^{V}O)(PO_4)_2$ (tetragonal, *a* = 8.6313(6) Å, *c* = 9.0211(5) Å) was structurally characterized [43] and chosen for catalytic testing. Its crystal structure (Figure 5c and d) is closely related to that of vanadyl(IV)-silicophosphate $(V^{IV}O)Si(PO_4)_2$ [41,42], though not isotypic. The vanadium-oxygen substructure is described by chains of trans-vertex sharing octahedra $[(V^{V}{=}O)O_5]$. Isomorphous substitution of P^{5+} by V^{5+} in $Fe^{III}_4(P_2O_7)_3$ (Figure 5a and b; [63] turned out to be possible over a wide compositional range according to $Fe^{III}_4[(P_{1-x}V_x)_2O_7]_3$ with $0 \le x \le 0.75$ [43]. For higher amounts of vanadium ($x > 0.5$), the formation of $(V_2O_7)^{4-}$ and $(PVO_7)^{4-}$ is also expected for this solid solution series.

Titanium-vanadium(V)-phosphates. In the system $TiO_{2.0}$ / $VO_{2.5}$ / $PO_{2.5}$ the new vanadyl(V)-titanium-phosphate $(V^{V}O)Ti_6(PO_4)_9$ ($P6_3/m$ (no. 176), *Z* = 2; *a* = 8.4438(3) Å, *c* = 22.215(1) Å) was structurally characterized [45,46]. Its crystal structure (Figure 6a) contains $[Ti^{IV}_2O_9]$ double-octahedra and distinct $(V^{V}{=}O)^{3+}$ groups and is related to that of NASICON-type phosphates like $NaZr_2(PO_4)_3$ [64] and to the “empty NASICONs”

like $Nb^{IV}Nb^{V}(PO_4)_3$ [65] and $V^{IV}Nb^{V}(PO_4)_3$ ([49], Figure 6b). In marked contrast to these structures as well as to all other oxo-compounds of vanadium(V) the structure contains $(V{=}O)^{3+}$ groups, which are coordinated by three phosphate anions. This structural feature may be described as a strongly distorted $(V{=}O)O_3$ tetrahedron with one very short (terminal) bond at d(V-O) = 1.56 Å and three longer (bridging) bonds at d(V-O) ≈ 1.70 Å [45,46]. The structural similarity to $(V{=}O)O_3$ groups on a silica support [66,67] is striking and triggered our interest in the catalytic properties of this compound. In a similar way as it is observed for iron(III) pyrophosphate, substitution of P^{5+} by V^{5+} is possible [45,46] in TiP_2O_7 (Figure 7c; [68,69] according to $Ti(P_{1-x}V_x)_2O_7$). However, the upper solubility limit was determined at x = 0.43 [45,46], thus giving only rise to the formation of $(PVO_7)^{4-}$ groups besides $(P_2O_7)^{4-}$ groups. For the isotypic solid solution $Zr(P_{1-x}V_x)_2O_7$ complete miscibility has been reported [47]. In addition, in the system $ZrO_{2.0}$ / $VO_{2.5}$ / $PO_{2.5}$ partial substitution of P^{5+} by V^{5+} in the orthorhombic modification of $Zr_2O(PO_4)_2$ [48] was found [45]. No evidence for the substitution of Zr^{4+} cations, which occur in the structure in a pentagonal-bipyramidal coordination by oxygen to V^{5+}, was found. The last structure to be described (Figure 7a) is that of T-Nb_2O_5, a metastable form of niobia [51]. Synthetic experiments aiming at VNb_9O_{25} and $(V_{1-x}P_x)Nb_9O_{25}$, respectively, at rather low temperatures (ϑ = 450 °C) led to the formation of a homogeneous powder which showed an XRPD pattern very similar to that of T-Nb_2O_5. As basis for its structural description we are using the structure of the isotypic but crystallographically better characterized mixed oxide $W_6Ta_{74}O_{203}$ [70]. Twelve out of 16 niobium atoms in the unit cell show a pentagonal-bipyramidal coordination, while the remaining four are octahedrally coordinated. We believe that these might have been substituted for vanadium.

3.2 Structure and catalytic properties

During our investigation of the catalytic properties of vanadyl(IV)-, vanadyl(V)-, and vanadate(V)-phosphates, five new compounds, $AgV^{IV,V}{}_2P_{1.6}O_{7+\delta}$ (related to $Ag_6(V^{IV}O)_2(PO_4)_2(P_2O_7)$, Figure 2b [34]); $(V^{IV}O)_2[B(OH)_4](PO_4)$, Figure 3a and b [38], $V^{III}[B_2P_2O_7(OH)_5]$, Figure 4 [38]; $Fe(V^{V}O)(PO_4)_2$, Figure 5c and d [43]; $(V^{V}O)Ti_6(PO_4)_9$, Figure 6a [45,46], were synthesized and structurally characterized. Furthermore, the hitherto unknown solid solutions $Fe^{III}{}_4[(P_{1-x}V_x)_2O_7]_3$ ($0 \le x \le 0.75$), $Ti(P_{1-x}V_x)_2O_7$ ($0 \le x \le 0.43$), $(P_{1-x}V_x)Nb_9O_{25}$ ($0 \le x \le 1$), and $Zr_2O[(P_{1-x}V_x)O_4]_2$ ($0 \le x \le 0.07$) were obtained and their lattice parameters determined. All of these vanadium-containing compounds comply with the generally accepted chemical and structural requirements (as described in the "Introduction") for selective oxidation catalysts. Nevertheless, the materials' chemical

compositions and structural features are quite different. In addition to the new compounds, the already known phases $Ag(V^{IV}O)(V^{V}O)(PO_4)_2$ [65], $V^{III}_2[BP_3O_{12}]$ [39], ZrV_2O_7 [47], $V^{IV}Nb^{V}(PO_4)_3$ [49], and members of the solid solution series $Zr(P_{1-x}V_x)_2O_7$ were synthesized and tested for their catalytic behaviour. In total 29 vanadium-containing catalyst materials were investigated. Some possess the same overall chemical composition, but exhibit different crystallinity (specific surface) and phase composition due to varied temperature treatments, *e.g.* heating at low temperature around 400 to 450 °C or low-temperature pre-reaction followed by sintering at higher temperatures (700 to 1050 °C; Table 1).

The optical basicity Λ_o of a catalyst material has been suggested to be correlated with its selectivity in mild oxidation catalysis of hydrocarbons [13,14]. According to this concept, put forward by BORDES-RICHARD and COURTINE [13,14], the optical basicity of a solid should be one (out of several) descriptor(s) for its behaviour as catalyst in the selective oxidation. Optical basicities calculated for the materials under investigation (Table 3) using the data given by LEBOUTEILLER and COURTINE [71] are in the range $0.41 \leq \Lambda_o \leq 0.70$, with $(V^{IV}O)_2[B(OH)_4](PO_4)$ forming the lower and ZrV_2O_7 the upper limit. This range also comprises $\Lambda_o\{(VO)_2P_2O_7\} = 0.49$ and Λ_o(MoVNbTeO; *M1* phase) = 0.64 [71], the only materials discovered so far to show excellent performance in selective oxidation of *n*-butane to MA.

Despite this compliance, the majority of compounds included in our study did not show any selectivity for oxidation of *n*-butane to MA (Table 2). The best result was obtained for Cat-1, with the approximate composition $Ag_2V^{4.1+}P_{1.6}O_{7.05}$ and (according to its XRPD pattern) with a structure closely related to $Ag_6(V^{IV}O)_2(PO_4)_2(P_2O_7)$ [34]. In total, only twelve out of 29 materials showed minimal selectivity for MA (Table 2). Apart from Cat-1, only Cat-3, Cat-13, and Cat-17 showed activity and MA selectivity (Table 2). Cat-3, $(V^{IV}O)_2[B(OH)_4][PO_4]$, however, is unstable under reaction conditions (Table 2), and the observed catalytic effect is likely to be related to the formed decomposition products.

Cat-13, which is amorphous "$(V^{V}O)Ti_6(PO_4)_9$", remains amorphous under testing conditions. Results of MAS-NMR spectroscopy (^{31}P and ^{51}V nuclei) show the presence of pre-crystalline $Ti_5O_4(PO_4)_4$ and β-$VOPO_4$, and small amounts of $VOPO_4 \cdot 2H_2O$ / α_I-$VOPO_4$ [45,46]. The dihydrate and the α_I-phase show similar chemical shifts in ^{31}P-MAS-NMR and are difficult to distinguish. Furthermore, α_I-$VOPO_4$, which is likely to be present in the catalyst at the temperatures considered, is quite hygroscopic and transforms upon uptake of water into the dihydrate. Therefore, the catalytic effect observed for Cat-13 does not originate from $(V^{V}O)Ti_6(PO_4)_9$, but is probably related to the amounts of $VOPO_4 \cdot 2H_2O$ / α_I-$VOPO_4$ present in the catalyst material. Well crystallized

$(V^{V}O)Ti_6(PO_4)_9$ (Cat-14) shows much lower activity and a low selectivity for MA. The lower activity might be linked to the significantly lower specific surface of the sintered material.

Amorphous $Ti(P_{0.6}V_{0.4})_2O_7$, a member of the V-rich solid solution (Cat-17), shows quite high activity, but only poor selectivity for MA. By MAS-NMR (^{31}P, ^{51}V) pre-crystalline β-$VOPO_4$ and $Ti(P_{0.6}V_{0.4})_2O_7$ were identified as components of the catalyst, which remains amorphous under testing conditions.

Vanadium substituted zirconium phosphates (Cat-19 to Cat-24) act as total oxidation catalysts. They all are stable under the testing conditions. The significantly higher activity of $Zr(P_{0.5}V_{0.5})_2O_7$ in comparison to the pure vanadate is quite remarkable. We attribute this effect to the significantly lower nucleophilicity (optical basicity) of the mixed phosphate-vanadate, which is in agreement with the reasoning of BORDES [13]. We can explain the high activity of the vanadium-substituted zirconium-oxide-phosphate (Cat-23 and Cat-24), which has even lower vanadium content, in a similar way.

Metastable *T*-Nb_2O_5 (Cat-25 and Cat-27), which possibly contains some V^{5+} at octahedral sites (see Section 3), is a highly active combustion catalyst, even if the vanadium content is further lowered due to the overall composition "$(P_{0.5}V_{0.5})Nb_9O_{25}$". The well crystallized samples VNb_9O_{25} and $(P_{0.5}V_{0.5})Nb_9O_{25}$ show much lower catalytic activity, as it was also observed for the various well-crystallized zirconium-phosphate-vanadates. This effect might be related to a lower surface area caused by sintering during crystallization.

The various catalyst materials of the system Fe_2O_3 / V_2O_5 / P_2O_5 (Cat-7 to Cat-12) show optical basicities (Table 3) in the range of $(VO)_2P_2O_7$ and "MoVNbTe (*M1* phase)". In addition, the structural features required for an oxidation catalyst, *i.e.* linkage of MO_n polyhedra and (for $Fe(V^{V}O)(PO_4)_2$) the presence of $(V{=}O)^{3+}$ groups, was observed. Nevertheless, the other iron vanadium phosphates were relatively inactive catalysts. The only exception, *viz.* the very highly active amorphous Cat-11, is probably due to the presence of V_2O_5 as a result of incomplete equilibration at the rather low reaction temperature.

$VOPO_4$ [72] and V_2O_5 [73], which contain purely pentavalent vanadium as $(V{=}O)^{3+}$ or $(O{=}V{=}O)^{+}$ units, are fairly active catalyst materials, which favour oxidation of alkanes to CO_x. With respect to this catalytic behaviour, it is quite interesting to note that compounds like $Ag(V^{IV}O)(V^{V}O)(PO_4)_2$ (Cat-2), $Fe(V^{V}O)(PO_4)_2$ (Cat-8), and $(V^{V}O)Ti_6(PO_4)_9$ (Cat-14) are almost inactive catalyst materials.

3.2 Electronic properties

As shown above, the correlation of crystallographic properties, like the presence of distinct structural building blocks in the crystal structure of the bulk catalysts, and the catalytic performance is not straightforward. Hence we have developed a new method that allows the measurement of the charge transfer properties of the working catalysts in order to include the electronic properties of the catalyst as an important criterion for the catalytic behaviour in selective oxidation reactions. The newly established noncontact microwave conductivity method was applied to investigate the selective oxidation of *n*-butane to maleic anhydride on the bulk reference catalyst vanadyl pyrophosphate (VPO) and the new catalytically active compound $Ag_2V^{IV,V}P_{1.6}O_{7+\delta}$ (Cat-1) between room temperature and 400 °C in different gas atmospheres. Figure 8 shows that the conductivity of the samples under isothermal conditions at 400 °C varies strongly in dependence on the surrounding gas phase chemical potential. Both catalysts exhibit the behaviour of a p-type semiconductor with increased conductivity under oxidizing, and reduced conductivity under reducing gas atmospheres. The fundamental difference between the two catalysts is their dynamic behaviour under reaction conditions. As for the highly selective and active VPO catalyst (*n*-butane conversion at 400 °C: ca. 50%, MA selectivity: ca. 80% as measured by the *in situ* MCPT/GC setup), the conductivity is smallest under selective catalytic conditions and increases upon reoxidation (Figure 8a). The observed conductivity rise in *n*-butane/N_2 is due to the formation of strongly conductive coke as proven by *in situ* Raman spectroscopy. The data compare well with corresponding ambient pressure photoelectron spectroscopy experiments [30]. Advanced studies even prove a monotonic correlation between the rate of maleic anhydride formation and conductivity upon changing the reaction gas contact time [30]. Although the less active sample Cat-1 (*n*-butane conversion at 400 °C: ca. 5%, MA selectivity: ca. 30% as measured by the *in situ* MCPT/GC setup) exhibits a significantly larger absolute conductivity than VPO, changes are only observed under oxidizing (in air) or strongly reducing conditions (*n*-butane in N_2) (Figure 8b). In contrast, under lean reaction conditions the conductivity remains constant even after switching from oxidizing to reaction gas mixtures. Moreover the conductivity does not remain stable in an inert gas atmosphere. Inactive crystalline and phase-pure samples such as $(V^{IV}O)(PO_3)_2$ do not show any systematic response under oxidizing, reducing or reaction conditions. This suggests that the method can detect active samples. The dynamic conductivity of VPO can be explained by a strong electronic interaction between gas molecules bound to surface states and the bulk by the formation of a sub-surface space charge layer as in an electrical gas sensor (chemiresistor) [30]. This effect can be interpreted in terms of charge transfer

along the $[V_2O_4]$-chains of crystalline VPO terminating at the surface with (100) orientation indicating the peculiar relation between the structural, electronic and catalytic properties of VPO. Although the Cat-1 sample does react as chemiresistor under strongly reducing or oxidizing conditions as well, a pronounced charge transfer is obviously hampered under the chemical potential set by the lean reaction gas mixture.

4 Conclusions

The application of new synthesis concepts yielded the identification of silver-vanadium phosphate of approximate composition $Ag_2V^{IV,V}P_{1.6}O_{7+\delta}$ ($0 \leq \delta \leq 0.5$) as catalyst in the selective oxidation of *n*-butane to maleic anhydride with the potential for further optimization. We have, however, shown that the catalytic performance of $(VO)_2P_2O_7$ based catalysts cannot be surpassed by any of the new structures evaluated in the present work so far. The synthesis of a broad variety of crystal structures guided by predictions discussed in literature did not yield an unambiguous correlation between the presence of specific structural units within the crystal structure or the site isolation on the surface caused by structural arrangements and catalytic activity and selectivity. The charge transfer properties and the bulk-surface interaction of the synthesized catalysts were included as complementary optimization parameters. For this purpose, we developed a contact-free method to probe the electrical conductivity of powder catalysts in a fixed-bed flow-through reactor under working conditions based on the microwave cavity perturbation technique and combined the method with *in situ* photoelectron spectroscopic investigations. The results of the measurements provide an explanation for the excellent catalytic behaviour of VPO catalysts and enable the identification of new reference variables in the search for new catalysts. VPO shows a peculiar dynamic behaviour like an electrical gas sensor in oxidizing, reducing and lean reaction gas atmospheres. In contrast, the conductivity of the less active $Ag_2V^{IV,V}P_{1.6}O_{7+\delta}$ catalyst does not respond to the reaction gas mixture, suggesting a hindered charge transfer under these conditions. The redox processes on the surface of VPO are completely reversible and restricted to the surface comprising a depth of 1-4 nm. The behaviour can be explained by including local surface states into the electronic description of the catalyst. A successful catalyst consists of a crystal structure that enables the formation of a flexible surface (mono-)layer that promotes the bulk-surface charge transfer. The latter parameter can be measured by the microwave cavity perturbation technique developed

within the present work, which represents a major step forward to monitor, predict, and finally rationally design materials with optimized catalytic performance in view of improved resource efficiency in industrially highly relevant reactions, such as the selective oxidation of alkanes.

Acknowledgments

The authors acknowledge valuable contributions of Patrick Hubach (BASF SE), Dr. W. Hoffbauer, Dr. M. S. Islam, Dr. K. Panagiotidis, Dr. C. Litterscheid, R. Groher, K. Wittich, and T. Freers (all Bonn University), J. Jentsch, P. Marasas, Dr. H. Borrmann and Dr. Y. Prots (all MPI CPfS).

The financial support of the BMBF project “ReAlSelOx” (033R028) is gratefully acknowledged.

Symbols used

$X_{n\text{-butane}}$ [%]	*n*-butane conversion
S_{MA} [mol-%]	selectivity to maleic anhydride
S_{COx} [mol-%]	selectivity to CO_2 and CO
T [°C]	reaction temperature of *n*-butane oxidation
$C_{n\text{-butane}}$ [vol-%]	volume concentration of *n*-butane in reaction gas inlet
Λ	optical basicity
CN	coordination number

References

[1] F. Cavani, *Catal. Today* **2010**, *157*, 8.

[2] R. I. Bergman, N. W. Frisch, *US Patent 3 293 268*, **1966**.

[3] G. Centi, F. Trifiro, J. R. Ebner, V. M. Franchetti, *Chem. Rev.* **1988**, *88*, 55.

[4] K. Weissermel, H.-J. Arpe, *Industrielle Organische Chemie*, 3. Auflage, VCH Verlagsgesellschaft mbH, Weinheim **1988**.

[5] N. Ballarini, F. Cavani, C. Cortelli, S. Ligi, F. Pierelli, F. Trifiro, C. Fumagalli, G. Mazzoni, T. Monti, *Top. Catal.* **2006**, *38*, 147.

[6] R. K. Grasselli, *Catal. Today* **1999**, *49*, 141.

[7] P. A. Agaskar, R. K. Grasselli, D. J. Buttrey, B. White, *Stud. Surf. Sci. Catal.* **1997**, *110*, 219.

[8] R. Glaum, E. Benser, H. Hibst, *Chem. Ing. Tech.* **2007**, *79*, 843.

[9] E. Benser, R. Glaum, T. Dross, H. Hibst, *Chem. Mater.* **2007**, *19*, 4341.

[10] J. L. Callahan, R. K. Grasselli, *AIChE J.* **1963**, *9*, 755.

[11] J.-C. Volta, *Top. Catal.* **2001**, *15*, 121.

[12] B. K. Hodnett, *Heterogeneous Catalytic Oxidation*, John Wiley & Sons, Chichester (UK) **2000**.

[13] E. Bordes-Richard, *Top. Catal.* **2008**, *50*, 82.

[14] P. Moriceau, A. Lebouteiller, E. Bordes, P. Courtine, *PCCP* **1999**, *1*, 5735.

[15] M. E. Davis, C. J. Dillon, J. H. Holles, J. Labinger, *Angew. Chem.* **2002**, *114*, 886; *Angew. Chem. Int. Ed.* **2002**, *41*, 858.

[16] R. Schlögl, in *Modern Heterogenous Oxidation Catalysis* (Eds: N. Mizuno), Wiley-VCH, Weinheim **2009**.

[17] R. Schlögl, *Top. Catal.* **2011**, *54*, 627.

[18] H. Lux, *Z. Elektrochem.* **1939**, *45*, 303.

[19] H. Flood, T. Förland, *Acta Chem. Scand.* **1947**, *1*, 592.

[20] F. Cavani, G. Centi, F. Trifiro, R. K. Grasselli, presented at *ACS Symposium of Division of Petroleum Chemistry, "Hydrocarbon Oxidation"*, New Orleans, September **1987**.

[21] V. A. Zazhigalov, A. I. Pyatnitskaya, I. V. Bacherikova, G. A. Komashko, G. Ladwig, V. M. Belousov, *React. Kinet. Catal. Lett.* **1983**, *23*, 119.

[22] A. S. Borovik, *Chem. Soc. Rev.* **2011**, *40*, 1870.

[23] X. Rozanska, R. Fortrie, J. Sauer, J. Phys. Chem. **2007,** C111*,* 6041.

[24] M. A. Pepera, J. L. Callahan, M. J. Desmond, E. C. Milberger, P. R. Blum, N. J. Bremer, *J. Am. Chem. Soc.* **1985**, *107*, 4883.

[25] M . Abon, K. E. Bere, P. Delichere, *Catal. Today* **1997**, *33*, 15.
[26] U. Rodemerck, B. Kubias, H. W. Zanthoff, M. Baerns, *Appl. Catal. A* **1997**, *153*, 203.
[27] D. X. Wang, H. H. Kung, M. A. Barteau, *Appl. Catal. A* **2000**, *201*, 203.
[28] M. J. Lorences, G. S. Patience, F. V. Diez, J. Costa, *Appl. Catal. A* **2004**, *263*, 193.
[29] R. K. Grasselli, *Top. Catal.* **2001**, *15*, 93-101.
[30] M. Eichelbaum, M. Hävecker, C. Heine, A. Karpov, C.-K. Dobner, F. Rosowski, A. Trunschke, R. Schlögl, *Angew. Chem. Int. Ed.* **2012**, *51*, DOI: anie.201201866 (in press).
[31] A. Karpov, C.-K. Dobner, R. Glaum, S.A. Schunk, F. Rosowski, *Chem. Ing. Techn.* **2011**, *83*, 1697.
[32] P. Ayyappan, A. Ramanan, C. C. Torardi, *Inorg. Chem.* **1998,** *37,* 3628.
[33] H.-Y. Kang, S.-L. Wang, P.-P. Tsai, K.-H. Lii, *J. Chem. Soc. Dalton Trans.* **1993**, *1993*, 1525.
[34] R. Glaum, K. Wittich, A. Karpov, A. Dobner, F. Rosowski, *unpublished results*, **2012**.
[35] A. Grandin, J. Chardon, M. M. Borel, A. Leclaire, B. Raveau, *J. Solid State Chem.* **1993**, *104*, 226.
[36] B. Ewald, Y.-X. Huang, R. Kniep, *Z. Anorg. Allg. Chem.* **2007**, *633*, 1517.
[37] Y. Taufiq-Yap, A. Hasbi, M. Hussein, G. Hutchings, J. Bartley, N. Dummer, *Catal. Lett.* **2006**, *106*, 177.
[38] F. Gruchow, *part of planned Ph.D. thesis*, MPI CPfS Dresden, **2012**.
[39] M. Meisel, M. Päch, L. Wilde, D. Wulff-Molder, *Z. Anorg. Allg. Chem.* **2004**, *630*, 983.
[40] I. Boy, C. Hauf, R. Kniep, *Z. Naturforsch., B: J. Chem. Sci.* **1998**, *53*, 631–633.
[41] N. Middlemiss, C. Calvo, *Acta Crystallogr.* **1976**, *B32*, 2896.
[42] C. E. Rice, W. R. Robinson, B. C. Tofield, *Inorg. Chem.* **1976**, *15*, 345.
[43] D. Vogt, V. Hiebert, R. Groher, K. Panagiotidis, R. Glaum, *unpublished results,* Univ. of Bonn **2012**,.
[44] K. K. Palkina, S. I. Maksimova, N. T. Chibiskova, K. Schlesinger, G. Ladwig, *Z. Anorg. Allg. Chem.* **1985**, *529*, 89.
[45] S. Titlbach, *part of planned Ph.D. thesis*, University of Bonn, **2012**.
[46] S. Titlbach, W. Hoffbauer, R. Glaum, *J. Solid State Chem.* **2012** submitted for publication.
[47] J. S. O. Evans, J. C. Hanson, A. W. Sleight, *Acta Crystallogr.* **1998**, *B54*, 705.

[48] W. Gebert, E. Tillmanns, *Acta Crystallogr.* **1975**, *B31*, 1768.
[49] P. A. Agaskar, R. K. Grasselli, D. J. Buttrey, B. White, US Patent Nr.: 5,354,722; **1994**.
[50] M. T. Casais, E. Gutierrez-Puebla, M. A. Monge, I. Rasines, C. Ruiz Valero, *J. Solid State Chem.* **1993***, 102*, 261.
[51] K. Kato, S. Tamura, *Acta Crystallogr.* **1975**, *B31*, 673.
[52] Y. Amemiya, J. Miyahara, *Nature* **1998**, *336*, 89.
[53] I. Tanaka, M. Yao, M. Suzuki, K. Hikichi, *J. Appl. Crystallogr.* **1990**, *23*, 334.
[54] K. Maaß, R. Glaum, R. Gruehn, *Z. Anorg. Allg. Chem.* **2002**, *626*, 1663.
[55] L.-F. Chen, C. K. Ong, C. P. Neo, V. V. Varadan, V. K. Varadan, *Microwave electronics: Measurement and materials characterization*, Wiley, 2004.
[56] M. Eichelbaum, R. Stößer, A. Karpov, C.-K. Dobner, F. Rosowski, A. Trunschke, R. Schlögl, *Phys. Chem. Chem. Phys.* **2012**, *14*, 1302.
[57] S. A. Schunk, D. Demuth, A. Cross, O. Gerlach, A. Haas, J. Klein, J. M. Newsam, A. Sundermann, W. Stichert, W. Strehlau, U. Vietze, T. Zech, "*Mastering the Challenges of Catalyst Screening in High-Throughput Experimentation for Heterogeneously Catalyzed Gas-phase Reactions"* in *High-Throughput Screening in Heterogeneous Catalysis*, Wiley-VCH, Weinheim, **2004**.
[58] M. Saupe, R. Födisch, A. Sundermann, S. A. Schunk, K.-E. Finger, *QSAR Comb. Sci.* **2005**, *24*, 66.
[59] R. Glaum, K. Wittich, A. Karpov, A. Dobner, F. Rosowski, *unpublished results*, **2012**.
[60] D. M. C. Huminicki, F. C. Hawthorne, *Can. Mineral.* **2002**, *40*, 923.
[61] R. Schlögl, *Concepts in Selective Oxidation of Small Alkane Molecules*, p. 32; in N. Mizuno (Ed.), *Modern Heterogeneous Oxidation Catalysis*, Wiley-VCH, Weinheim, **2009**.
[62] M. Tachez, F. Theobald, E. Bordes, *J. Solid State Chem.* **1981**, *40*, 280.
[63] L. K. Elbouaanani, B. Malaman, R. Gerardin, M. Ijjaali, *J. Solid State Chem.* **2002**, *163*, 412.
[64] L. O. Hagman, P. Kierkegaard, *Acta Chem. Scand.* **1968**, *22*, 1822.
[65] A. Leclaire, M. M. Borel, A. Grandin, B. Raveau, *Acta Crystallogr.* **1989**, *C45*, 699.
[66] R. G. Herman, Q. Sun, C. Shi, K. Klier, C.-B. Wang, H. Hu, I. E. Wachs, M. M. Bhasin, *Catal. Today* **1997**, *37*, 1.
[67] C. Pirovano, E. Schönborn, S. Wohlrab, V. Narayana Kalevaru, A. Martin, *Catal. Today* **2012**, doi:10.1016/j.cattod.2012.02.043.

[68] G. R. Levi, G. Peyronel, *Z. Kristallogr*. **1935**, *92*, 190.
[69] S. T. Norberg, G. Svensson, J. Albertsson, *Acta Crystallogr.* **2001**, C*57*, 225.
[70] S. Schmid, J. G. Thompson, A. D. Rae, B. D. Butler, R. L. Withers, *Acta Crystallogr.* **1995**, B*51*, 698.
[71] A. Lebouteiller, P. Courtine, *J. Solid State Chem.* **1998**, *137*, 94.
[72] M. Abon, K. E. Bere, A. Tuel, P. Delichere, *J. Catal.* **1995**, *156*, 28.
[73] K. Kourtakis, J. D. Sullivan, *WO Patent 98/13329*, **1998**.

Table 1. Summary of tested catalyst materials.

No.	Composition [a]	result of characterization [b] (before catalytic testing)	result of characterization [b] (after catalytic testing)
Cat-1	"$Ag_2V^{IV,V}P_{1.6}O_{7+\delta}$"	XRPD: similar to $Ag_6(V^{IV}O)_2(PO_4)_2(P_2O_7)$	not characterized
Cat-2	$Ag(V^{IV}O)(V^{V}O)(PO_4)_2$	XRPD: $Ag(V^{IV}O)(V^{V}O)(PO_4)_2$	XRPD: $Ag(V^{IV}O)(V^{V}O)(PO_4)_2$
Cat-3	$(V^{IV}O)_2[B(OH)_4][PO_4]$	XRPD: $(V^{IV}O)_2[B(OH)_4][PO_4]$	XRPD: V_2O_5, BPO_4, β-$VOPO_4$ [c]
Cat-4	$V[B_2P_2O_7(OH)_5]$	XRPD: $V[B_2P_2O_7(OH)_5]$	XRPD: V_2O_5, BPO_4, β-$VOPO_4$ [d]
Cat-5	$Fe_{0.5}V_{0.5}[B_2P_2O_7(OH)_5]$	XRPD: $Fe_{0.5}V_{0.5}[B_2P_2O_7(OH)_5]$	XRPD: $FePO_4$, BPO_4, β-$VOPO_4$
Cat-6	$V^{III}_2[BP_3O_{12}]$	XRPD: $V^{III}_2[BP_3O_{12}]$	not characterized
Cat-7	"$Fe(VO)(PO_4)_2$"	XRPD: amorphous	XRPD: amorphous
Cat-8	$Fe(VO)(PO_4)_2$	XRPD: $Fe(VO)(PO_4)_2$, traces of $FePO_4$	XRPD: $Fe(VO)(PO_4)_2$
Cat-9	"$Fe_4[(P_{0.9}V_{0.1})_2O_7]_3$"	XRPD: amorphous	XRPD: $FePO_4$
Cat-10	$Fe_4[(P_{0.9}V_{0.1})_2O_7]_3$	XRPD: $Fe_4[(P_{0.9}V_{0.1})_2O_7]_3$, traces of $FePO_4$	XRPD:$Fe_4[(P_{0.9}V_{0.1})_2O_7]_3$, traces of $FePO_4$
Cat-11	"$Fe_4[(P_{0.25}V_{0.75})_2O_7]_3$"	XRPD: amorphous	XRPD: amorphous
Cat-12	$Fe_4[(P_{0.25}V_{0.75})_2O_7]_3$	XRPD: $Fe_4[(P_{0.25}V_{0.75})_2O_7]_3$, traces of $FeVO_4$	XRPD:$Fe_4[(P_{0.25}V_{0.75})_2O_7]_3$, traces of $FeVO_4$
Cat-13	"$(VO)Ti_6(PO_4)_9$"	XRPD: amorphous; NMR: multi-phasic non-equilibrium mixture [e]	XRPD: amorphous
Cat-14	$(VO)Ti_6(PO_4)_9$	XRPD: $(VO)Ti_6(PO_4)_9$, traces of $Ti(P_{1-x}V_x)_2O_7$	XRPD: $(VO)Ti_6(PO_4)_9$, traces of $Ti(P_{1-x}V_x)_2O_7$
Cat-15	"$Ti(P_{0.8}V_{0.2})_2O_7$" P-rich	XRPD: amorphous; NMR: $Ti(P_{1-x}V_x)_2O_7$, β-$VOPO_4$, $Ti_5O_4(PO_4)_4$ [f]	XRPD: amorphous
Cat-16	$Ti(P_{0.8}V_{0.2})_2O_7$ P-rich	XRPD: P-rich $Ti(P_{1-x}V_x)_2O_7$	XRPD: P-rich $Ti(P_{1-x}V_x)_2O_7$
Cat-17	"$Ti(P_{0.6}V_{0.4})_2O_7$" V-rich	XRPD: amorphous; NMR: V_2O_5, β-$VOPO_4$, $Ti_5O_4(PO_4)_4$ [g]	XRPD: amorphous
Cat-18	$Ti(P_{0.6}V_{0.4})_2O_7$ V-rich	XRPD: V-rich $Ti(P_{1-x}V_x)_2O_7$	XRPD: V-rich $Ti(P_{1-x}V_x)_2O_7$
Cat-19	ZrV_2O_7	XRPD: ZrV_2O_7	XRPD: ZrV_2O_7
Cat-20	ZrV_2O_7	XRPD: ZrV_2O_7	XRPD: ZrV_2O_7
Cat-21	"$Zr(P_{0.5}V_{0.5})_2O_7$"	XRPD: $Zr(P_{0.5}V_{0.5})_2O_7$	XRPD: $Zr(P_{0.5}V_{0.5})_2O_7$
Cat-22	$Zr(P_{0.5}V_{0.5})_2O_7$	XRPD: $Zr(P_{0.5}V_{0.5})_2O_7$	XRPD: $Zr(P_{0.5}V_{0.5})_2O_7$
Cat-23	"$Zr_2O[(P_{0.95}V_{0.05})O_4]_2$"	XRPD: $Zr_2O[(P_{0.95}V_{0.05})O_4]_2$	$Zr_2O[(P_{0.95}V_{0.05})O_4]_2$ monoclinic

		monoclinic	
Cat-24	$Zr_2O[(P_{1-x}V_x)O_4]_2$	XRPD: $Zr_2O(PO_4)_2$ orthorhombic	XRPD: $Zr_2O(PO_4)_2$ orthorhombic
Cat-25	"VNb_9O_{25}"	XRPD: *T*-Nb_2O_5 [51] broad reflections	XRPD: *T*-Nb_2O_5 [51] broad reflections
Cat-26	VNb_9O_{25}	XRPD: VNb_9O_{25}	XRPD: VNb_9O_{25}
Cat-27	"$(V_{0.5}P_{0.5})Nb_9O_{25}$"	XRPD: *T*-Nb_2O_5 [51] broad reflections; ^{31}P-MAS-NMR: δ_{iso} = -16.1 ppm	XRPD: *T*-Nb_2O_5 [51] broad reflections
Cat-28	$(V_{0.5}P_{0.5})Nb_9O_{25}$	XRPD: $(V_{0.5}P_{0.5})Nb_9O_{25}$; ^{31}P-MAS-NMR: δ_{iso} = -16.1 ppm	$(V_{0.5}P_{0.5})Nb_9O_{25}$
Cat-29	"$V^{IV}Nb^{V}(PO_4)_3$"	XRPD: amorphous	XRPD: amorphous

a) Compositions given in parentheses refer to overall chemical compositions only; in contrast formula without parentheses refer to a particular phase of given composition.

b) X-ray powder diffraction (XRPD; Guinier method and powder diffractometry; see section 2.2 and MAS-NMR spectroscopy using ^{31}P and ^{51}V nuclei have been used for characterization.

c) At testing conditions with higher amounts of *n*-butane in the gas mixture the starting material $(V^{IV}O)_2[B(OH)_4][PO_4]$ was stable

d) At testing conditions with higher amounts of *n*-butane in the gas mixture the starting material $V^{III}[B_2P_2O_7(OH)_5]$ was oxidized to $V^{III}V^{IV}{}_3O_3(PO_4)_3$ and BPO_4.

e) By ^{31}P- and ^{51}V-MAS-NMR spectroscopy pre-crystalline forms of β-$VOPO_4$ and $VOPO_4{\cdot}2H_2O/\alpha_I$-$VOPO_4$ (see text) are clearly indicated. As titanium-containing intermediate pre-crystalline $Ti_5O_4(PO_4)_4$ and, possibly, smaller amounts of $Ti(P_{1-x}V_x)_2O_7$ and/or $(VO)Ti_6(PO_4)_9$ are present. Due to similar range of chemical shift in ^{31}P-MAS-NMR [45,46] a clear distinction between the three phases in the amorphous material is impossible.

f) According to ^{31}P- and ^{51}V-MAS-NMR spectra the non-equilibrium mixture consists of pre-crystalline $Ti(P_{1-x}V_x)_2O_7$, β-$VOPO_4$ and $VOPO_4{\cdot}2H_2O/\alpha_I$-$VOPO_4$ (see text), and as additional titanium-containing phase pre-crystalline $Ti_5O_4(PO_4)_4$ and/or small amounts of $(VO)Ti_6(PO_4)_9$. Due to similar range of chemical shift in ^{31}P-MAS-NMR [45,46] a clear distinction between the three titanium-containing phases in the amorphous material is impossible.

g) According to ^{31}P- and ^{51}V-MAS-NMR spectra the amorphous V-rich $Ti(P_{1-x}V_x)_2O_7$ non-equilibrium mixture consists of pre-crystalline V_2O_5, β-$VOPO_4$ and small amounts of $VOPO_4{\cdot}2H_2O/\alpha_I$-$VOPO_4$. As titanium-containing phase pre-crystalline $Ti_5O_4(PO_4)_4$ was identified.

Table 2. Results of catalytic testing under various testing conditions.

No.	Composition	ϑ (°C)	$X_{n\text{-butane}}$ (%)	S_{MA} (%)	S_{COx} (%) $^{CO2+CO}$
Cat-1 [a)]	"$Ag_2V^{IV,V}P_{1.6}O_{7+\delta}$"	430	24	13	80+7
Cat-2	$Ag(V^{IV}O)(V^{V}O)(PO_4)_2$	380	5	-	100+0
Cat-3	$(V^{IV}O)_2[B(OH)_4][PO_4]$	400	18	17	39+44
Cat-4	$V[B_2P_2O_7(OH)_5]$	450	63	5	23+72
Cat-5	$Fe_{0.5}V_{0.5}[B_2P_2O_7(OH)_5]$	450	16	6	38+56
Cat-6	$V^{III}_2[BP_3O_{12}]$	420	8	24	30+46
Cat-7	"$Fe(VO)(PO_4)_2$"	420	7	-	45+55
Cat-8	$Fe(VO)(PO_4)_2$	420	-	-	-
Cat-9	"$Fe_4[(P_{0.9}V_{0.1})_2O_7]_3$"	420	14	-	40+60
Cat-10	$Fe_4[(P_{0.9}V_{0.1})_2O_7]_3$	420	7	-	67+33
Cat-11	"$Fe_4[(P_{0.25}V_{0.75})_2O_7]_3$"	420	80	-	35+65
Cat-12	$Fe_4[(P_{0.25}V_{0.75})_2O_7]_3$	420	14	-	47+53
Cat-13	"$(VO)Ti_6(PO_4)_9$"	350	26	23	32+45
Cat-14	$(VO)Ti_6(PO_4)_9$	350	8	15	40+45
Cat-15	"$Ti(P_{0.8}V_{0.2})_2O_7$" P-rich	350	7	41	0+59
Cat-16	$Ti(P_{0.8}V_{0.2})_2O_7$ P-rich	350	15	14	35+51
Cat-17	"$Ti(P_{0.6}V_{0.4})_2O_7$" V-rich	350	59	13	35+52
Cat-18	$Ti(P_{0.6}V_{0.4})_2O_7$ V-rich	350	3	17	54+29
Cat-19	ZrV_2O_7	420	24	-	44+56
Cat-20	ZrV_2O_7	420	18	-	46+54
Cat-21	"$Zr(P_{0.5}V_{0.5})_2O_7$"	420	67	-	38+62
Cat-22	$Zr(P_{0.5}V_{0.5})_2O_7$	420	32	-	38+62

Cat-23	"$Zr_2O[(P_{0.95}V_{0.05})O_4]_2$"	420	53	-	43+57
Cat-24	$Zr_2O[(P_{0.95}V_{0.05})O_4]_2$	420	47	-	40+60
Cat-25	"VNb_9O_{25}"	420	99	-	100+0
Cat-26	VNb_9O_{25}	420	18	-	64+36
Cat-27	"$(V_{0.5}P_{0.5})Nb_9O_{25}$"	420	98	-	99+1
Cat-28	$(V_{0.5}P_{0.5})Nb_9O_{25}$	420	18	-	94+6
Cat-29	"$V^{IV}Nb^{V}(PO_4)_3$"	380	20	5	59+36

a) Compositions given in parentheses refer to overall chemical compositions only; in contrast formula without parentheses refer to a particular phase of given composition (seeTable 1).
b) Feed composition: *n*-butane / air / H_2O = 1.85 / 95.15 / 3
c) Specific butane conversion rate: {gas flow [$nL \cdot h^{-1}$] × $C_{n\text{-butane}}$ [vol-%] / 100 × $X_{n\text{-butane}}$[%] / 100} / / {22.4 [$nL \cdot mol^{-1}$] × m_{cat} [g] × S_{cat} [$m^2 \cdot g^{-1}$]}
d) Feed composition: *n*-butane / air / H_2O = 2.1 / 94.9 / 3

Table 3. Optical basicity of tested vanadyl phosphates and vanadate-phosphates. For the calculation of Λ_o data from [71] have been used.

No.	compound	calculated Λ_o
Cat-1	$Ag_6(V^{IV}O)_2(PO_4)_2(P_2O_7)$	0.57
Cat-2	$Ag(V^{IV}O)(V^{V}O)(PO_4)_2$	0.52
Cat-3	$(V^{IV}O)_2[B(OH)_4][PO_4]$	0.50
Cat-4	$V^{III}[B_2P_2O_7(OH)_5]$	0.41
Cat-5	$Fe^{III}_{0.5}V^{III}_{0.5}[B_2P_2O_7(OH)_5]$	0.42 [a)]
Cat-6	$V^{III}_2[BP_3O_{12}]$	0.43 [a)]
Cat-8	$Fe(VO)(PO_4)_2$	0.49
Cat-10	$Fe_4[(P_{0.9}V_{0.1})_2O_7]_3$	0.51
Cat-12	$Fe_4[(P_{0.25}V_{0.75})_2O_7]_3$	0.65
Cat-14	$(VO)Ti_6(PO_4)_9$	0.49
Cat-16	$Ti(P_{0.8}V_{0.2})_2O_7$ (P-rich)	0.50
Cat-18	$Ti(P_{0.6}V_{0.4})_2O_7$ (V-rich)	0.55
Cat-20	ZrV_2O_7	0.70
Cat-22	$Zr(P_{0.5}V_{0.5})_2O_7$	0.57
Cat-23	$Zr_2O[(P_{0.95}V_{0.05})O_4]_2$	0.51
Cat-25	*T*-Nb_2O_5	0.61 [b)]
Cat-26	VNb_9O_{25}	0.61
Cat-28	$(V_{0.5}P_{0.5})Nb_9O_{25}$	0.60
Cat-29	$V^{IV}Nb^{V}(PO_4)_3$	0.45

a) $\Lambda_o(V_2O_3)$ used in the calculation has been chosen to be equal to $\Lambda_o(Cr_2O_3) = 0.70$.
b) $\Lambda_o(Nb_2O_5) = 0.70$ for Nb^{5+} in octahedral coordination.

Figure Legends

Figure 1. Schematic of the *in situ* MCPT/on line GC setup to measure simultaneously catalytic performance data and electrical conductivity of polycrystalline catalysts in a fixed-bed flow-through reactor. The network analyzer includes the microwave source and detector for the measurement.

Figure 2. Vanadyl-phosphate layers $[V^{V}O_2PO_4]^{2-}$ in $Ag_2(V^{V}O_2)(PO_4)$ [33] (a) and $[(V^{IV}O)_2(PO_4)_2(P_2O_7)]^{6-}$ in $Ag_6(V^{IV}O)_2(PO_4)_2(P_2O_7)$ [59] (b) and tetramers $[V^{IV}{}_2V^{V}{}_2O_{20}]$ in $Ag(V^{IV}O)(V^{V}O)(PO_4)_2$ [35] (c). VO_6: dark-grey, P_2O_7: grey, PO_4: light-grey, Ag^+: grey spheres.

Figure 3. Comparison of the crystal structures of $(V^{IV}O)_2[B(OH)_4][PO_4]$ [38] (a, b) and α_I-$V^{V}OPO_4$ [61] (c, d). VO_6: dark-grey, tetrahedra $B(OH)_4$ and PO_4: white, the unit cells for the two structures are indicated.

Figure 4. Crystal structure of $V^{III}[B_2P_2O_7(OH)_5]$ [38]. $[VO_6]$: grey, $BO_2(OH)(OH_{0.5})$: dark-grey, $PO_3(OH)$: white.

Figure 5. Crystal structures of $Fe^{III}{}_4(P_2O_7)_3$ [63] (a, b; FeO_6: dark-grey, PO_4: light-grey) and of $Fe(V^{V}O)(PO_4)_2$ [43] (c, d; VO_6: dark-grey, FeO_4: grey, PO_4: light-grey).

Figure 6. Crystal structures of $(V^{V}O)Ti_6(PO_4)_9$ [45,46] (a) and of "$VNb(PO_4)_3$" [49] (b). MO_6: dark-grey (*M*: Ti, V, Nb), PO_4: light-grey, $(V{=}O)O_3$: grey.

Figure 7. Crystal structures of *T*-Nb_2O_5 with NbO_7 (grey) and NbO_6 (dark-grey) groups [51] (a), *o*-$Zr_2O(PO_4)_2$ with ZrO_7 (dark-grey) and PO_4 (light-grey) polyhedra [48] (b), and TiP_2O_7 with TiO_6 (grey) and P_2O_7 (light-grey) groups [68,69] (c).

Figure 8. Microwave conductivity and temperature program for VPO (a) and $Ag_2V^{IV,V}P_{1.6}O_{7+\delta}$ (b) between 20 and 400 °C in 2% *n*-butane/20% O_2 (C4/O2), 20% O_2 (O2), 100% N_2 (N2) and 2% *n*-butane (C4), residual gas is always N_2.

Short text for the table of contents section

Novel vanadium-phosphates containing vanadium atoms in different oxidation states are investigated as catalysts for *n*-butane oxidation.

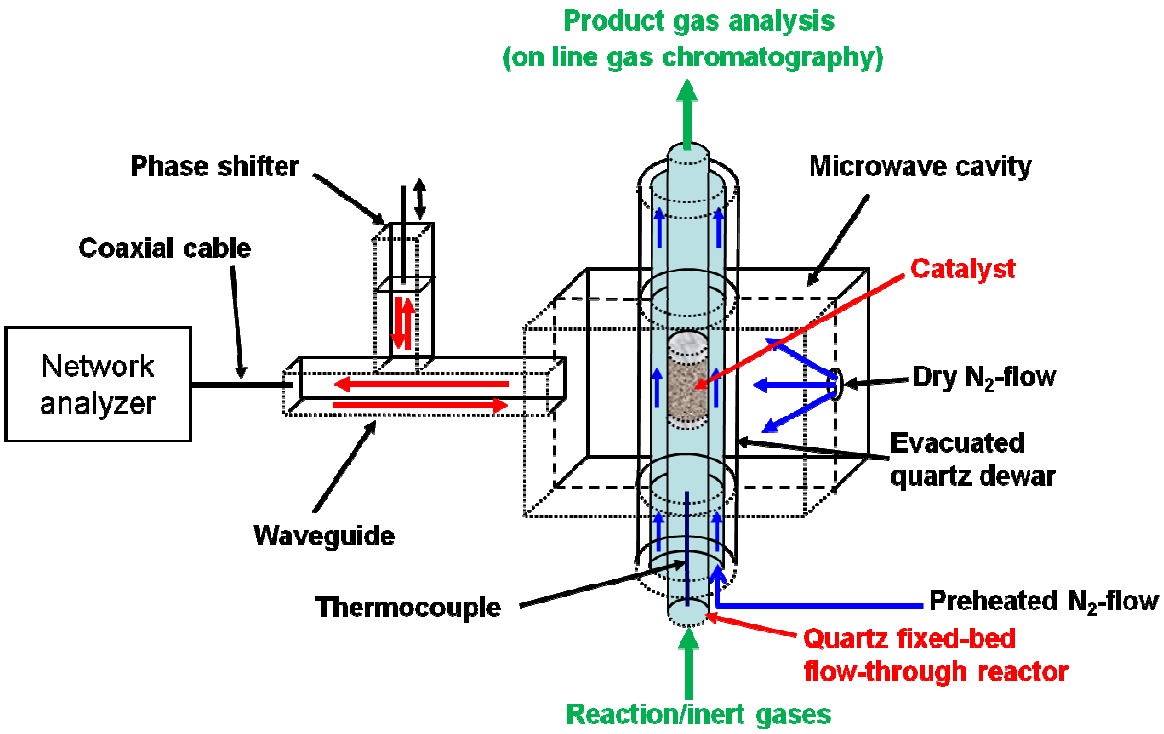
Product gas analysis
(on line gas chromatography)
Phase shifter
Microwave cavity
Coaxial cable
Catalyst
Network analyzer
Dry N_2-flow
Evacuated quartz dewar
Waveguide
Thermocouple
Preheated N_2-flow
Quartz fixed-bed flow-through reactor
Reaction/inert gases

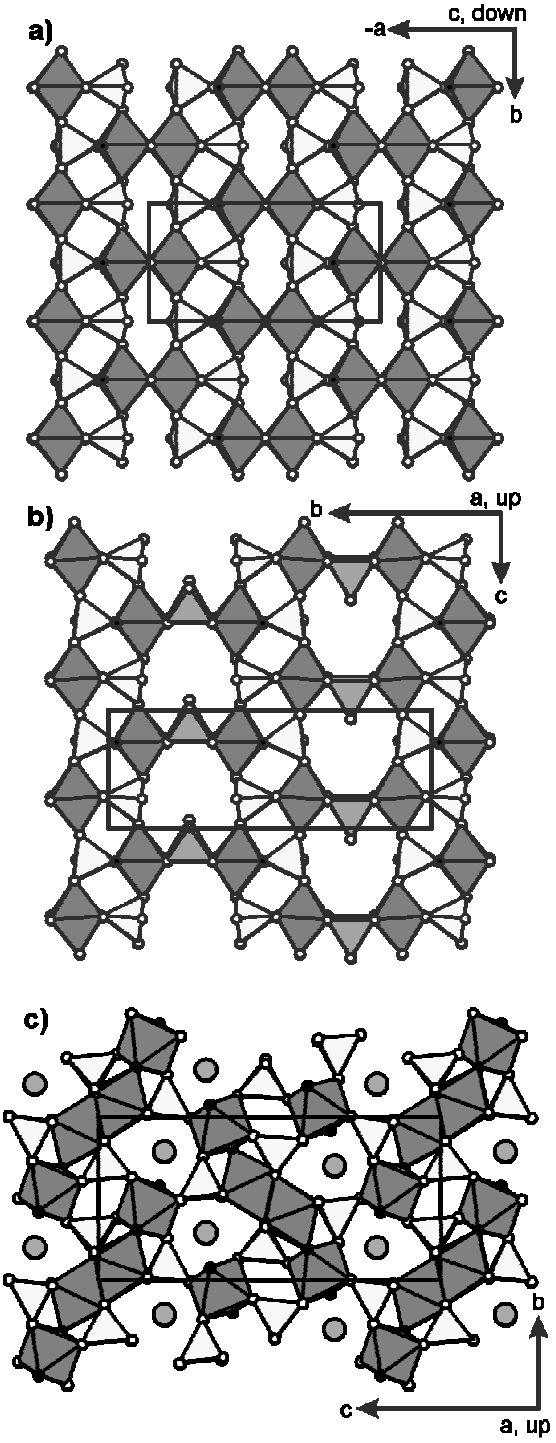
a)
-a
c, down
b
b)
b
a, up
c
c)
b
c
a, up

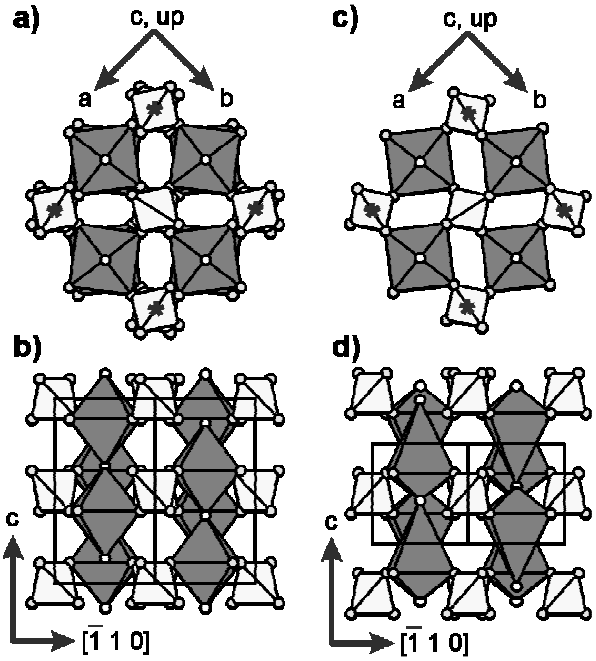
a)
c, up
a
b
c)
c, up
a
b
b)
c
[1̄ 1 0]
d)
c
[1̄ 1 0]

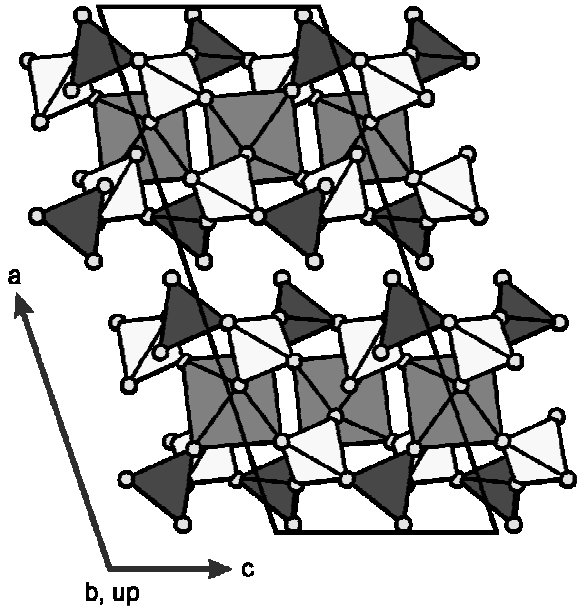
a
c
b, up

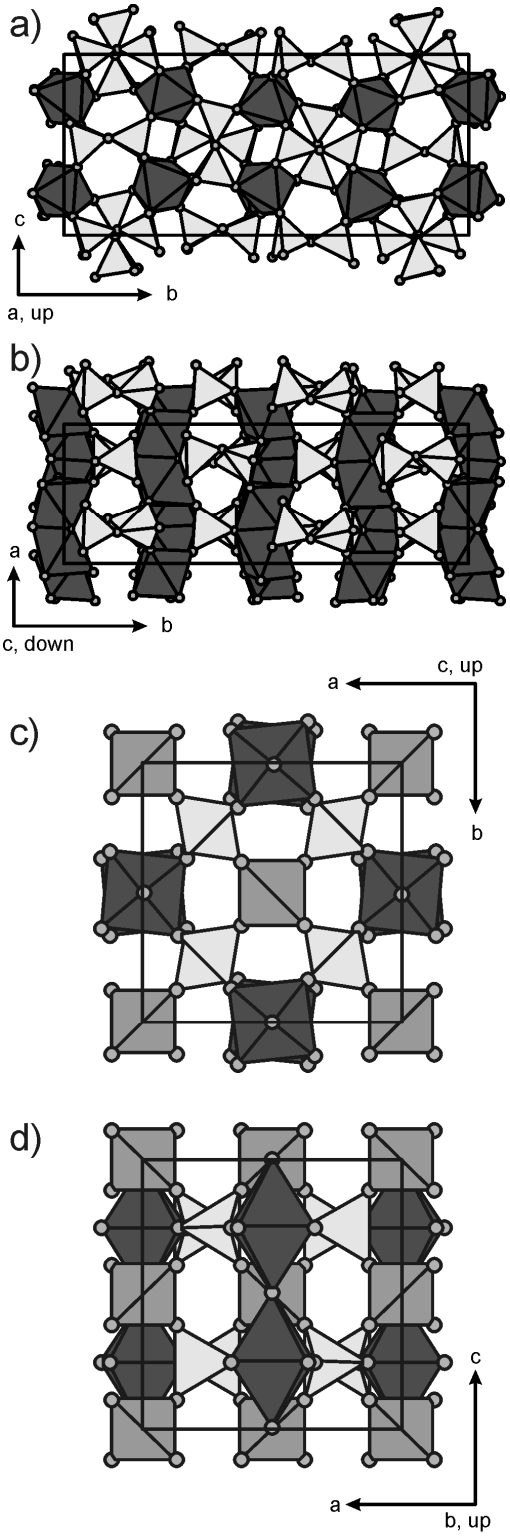
a)
c
b
a, up
b)
a
b
c, down
c)
a
c, up
b
d)
c
a
b, up

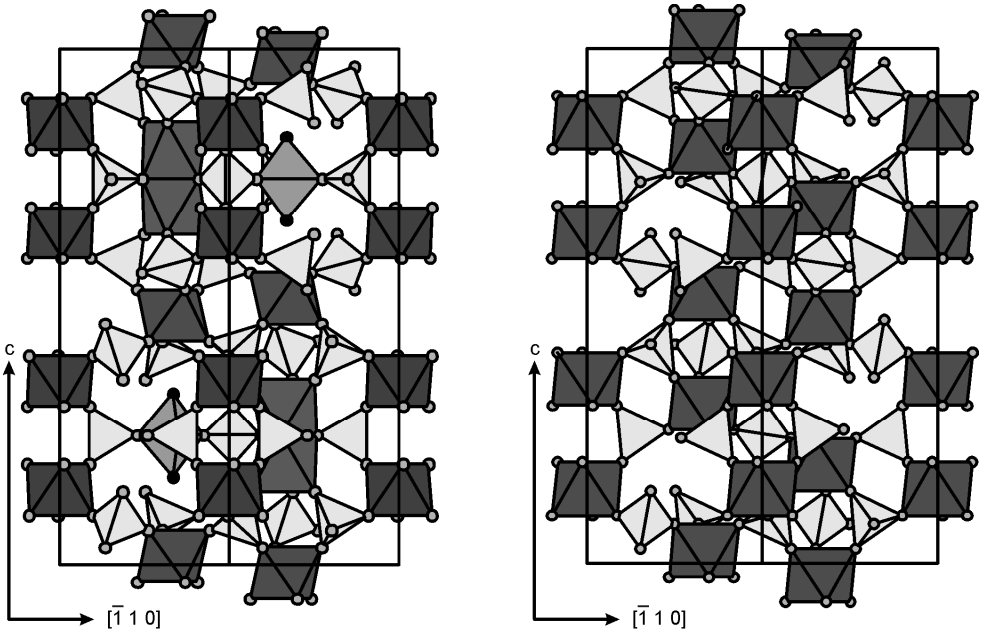
c
[$\bar{1}$ 1 0]
c
[$\bar{1}$ 1 0]

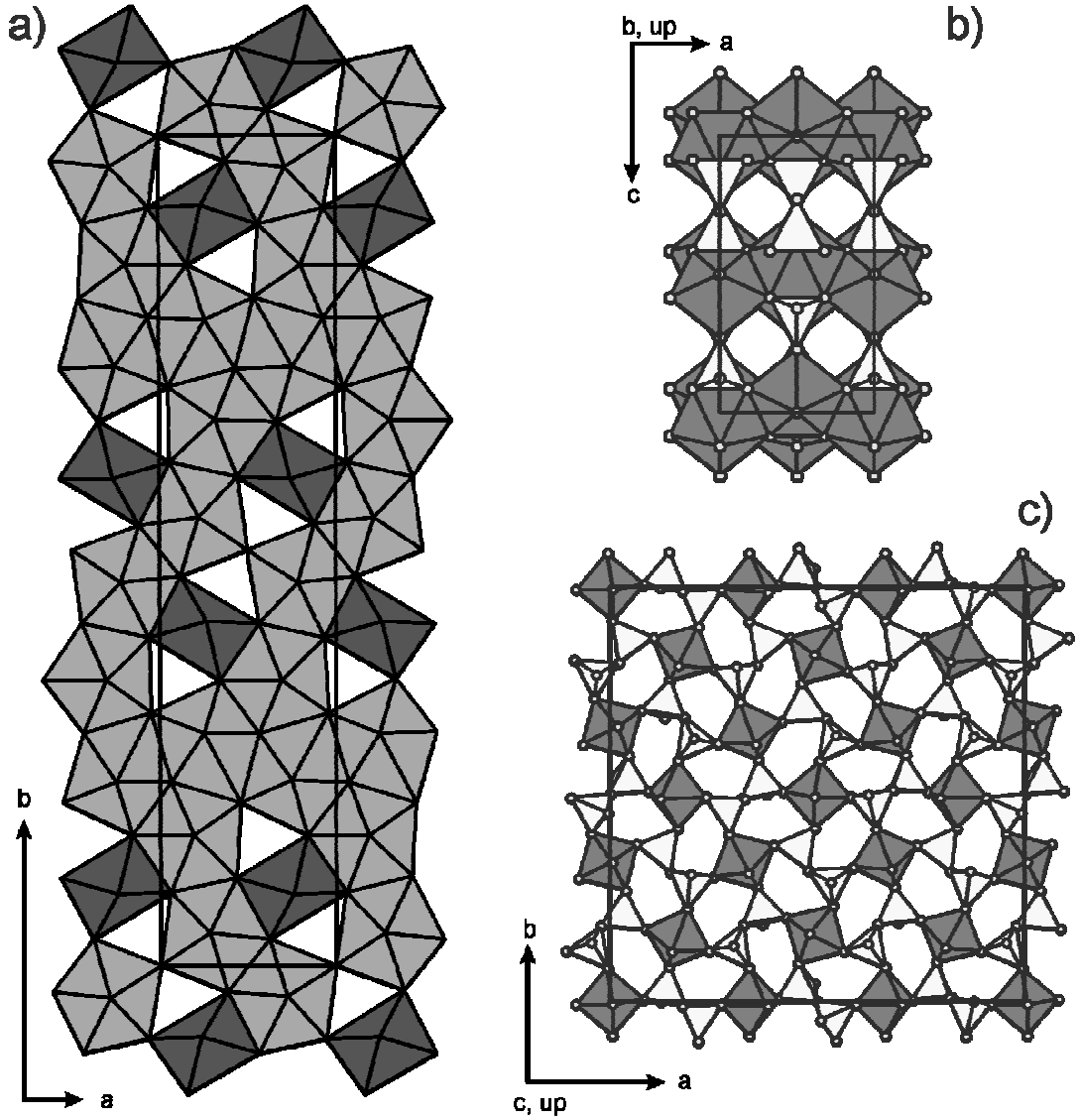
a)
b
a
b, up
a
c
b)
c)
b
a
c, up

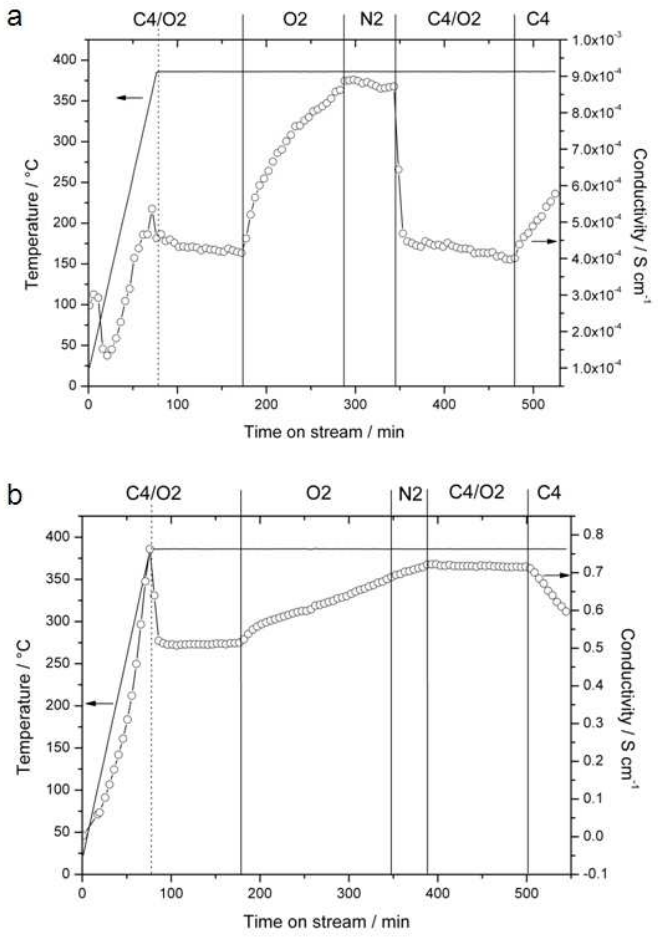
a
C4/O2
O2
N2
C4/O2
C4
Temperature / °C
Conductivity / S cm-1
Time on stream / min
b
C4/O2
O2
N2
C4/O2
C4
Temperature / °C
Conductivity / S cm-1
Time on stream / min

No.	Composition [a]	result of characterization [b] (before catalytic testing)	result of characterization [b] (after catalytic testing)
Cat-1	"$Ag_2V^{IV,V}P_{1.6}O_{7+\delta}$"	XRPD: similar to $Ag_6(V^{IV}O)_2(PO_4)_2(P_2O_7)$	not characterized
Cat-2	$Ag(V^{IV}O)(V^{V}O)(PO_4)_2$	XRPD: $Ag(V^{IV}O)(V^{V}O)(PO_4)_2$	XRPD: $Ag(V^{IV}O)(V^{V}O)(PO_4)_2$
Cat-3	$(V^{IV}O)_2[B(OH)_4][PO_4]$	XRPD: $(V^{IV}O)_2[B(OH)_4][PO_4]$	XRPD: V_2O_5, BPO_4, β-$VOPO_4$ [c]
Cat-4	$V[B_2P_2O_7(OH)_5]$	XRPD: $V[B_2P_2O_7(OH)_5]$	XRPD: V_2O_5, BPO_4, β-$VOPO_4$ [d]
Cat-5	$Fe_{0.5}V_{0.5}[B_2P_2O_7(OH)_5]$	XRPD: $Fe_{0.5}V_{0.5}[B_2P_2O_7(OH)_5]$	XRPD: $FePO_4$, BPO_4, β-$VOPO_4$
Cat-6	$V^{III}_2[BP_3O_{12}]$	XRPD: $V^{III}_2[BP_3O_{12}]$	not characterized
Cat-7	"$Fe(VO)(PO_4)_2$"	XRPD: amorphous	XRPD: amorphous
Cat-8	$Fe(VO)(PO_4)_2$	XRPD: $Fe(VO)(PO_4)_2$, traces of $FePO_4$	XRPD: $Fe(VO)(PO_4)_2$
Cat-9	"$Fe_4[(P_{0.9}V_{0.1})_2O_7]_3$"	XRPD: amorphous	XRPD: $FePO_4$
Cat-10	$Fe_4[(P_{0.9}V_{0.1})_2O_7]_3$	XRPD: $Fe_4[(P_{0.9}V_{0.1})_2O_7]_3$, traces of $FePO_4$	XRPD:$Fe_4[(P_{0.9}V_{0.1})_2O_7]_3$, traces of $FePO_4$
Cat-11	"$Fe_4[(P_{0.25}V_{0.75})_2O_7]_3$"	XRPD: amorphous	XRPD: amorphous
Cat-12	$Fe_4[(P_{0.25}V_{0.75})_2O_7]_3$	XRPD: $Fe_4[(P_{0.25}V_{0.75})_2O_7]_3$, traces of $FeVO_4$	XRPD:$Fe_4[(P_{0.25}V_{0.75})_2O_7]_3$, traces of $FeVO_4$
Cat-13	"$(VO)Ti_6(PO_4)_9$"	XRPD: amorphous; NMR: multi-phasic non-equilibrium mixture [e]	XRPD: amorphous
Cat-14	$(VO)Ti_6(PO_4)_9$	XRPD: $(VO)Ti_6(PO_4)_9$, traces of $Ti(P_{1-x}V_x)_2O_7$	XRPD: $(VO)Ti_6(PO_4)_9$, traces of $Ti(P_{1-x}V_x)_2O_7$
Cat-15	"$Ti(P_{0.8}V_{0.2})_2O_7$" P-rich	XRPD: amorphous; NMR: $Ti(P_{1-x}V_x)_2O_7$, β-$VOPO_4$, $Ti_5O_4(PO_4)_4$ [f]	XRPD: amorphous
Cat-16	$Ti(P_{0.8}V_{0.2})_2O_7$ P-rich	XRPD: P-rich $Ti(P_{1-x}V_x)_2O_7$	XRPD: P-rich $Ti(P_{1-x}V_x)_2O_7$
Cat-17	"$Ti(P_{0.6}V_{0.4})_2O_7$" V-rich	XRPD: amorphous; NMR: V_2O_5, β-$VOPO_4$, $Ti_5O_4(PO_4)_4$ [g]	XRPD: amorphous
Cat-18	$Ti(P_{0.6}V_{0.4})_2O_7$ V-rich	XRPD: V-rich $Ti(P_{1-x}V_x)_2O_7$	XRPD: V-rich $Ti(P_{1-x}V_x)_2O_7$
Cat-19	ZrV_2O_7	XRPD: ZrV_2O_7	XRPD: ZrV_2O_7
Cat-20	ZrV_2O_7	XRPD: ZrV_2O_7	XRPD: ZrV_2O_7
Cat-21	"$Zr(P_{0.5}V_{0.5})_2O_7$"	XRPD: $Zr(P_{0.5}V_{0.5})_2O_7$	XRPD: $Zr(P_{0.5}V_{0.5})_2O_7$
Cat-22	$Zr(P_{0.5}V_{0.5})_2O_7$	XRPD: $Zr(P_{0.5}V_{0.5})_2O_7$	XRPD: $Zr(P_{0.5}V_{0.5})_2O_7$
Cat-23	"$Zr_2O[(P_{0.95}V_{0.05})O_4]_2$"	XRPD: $Zr_2O[(P_{0.95}V_{0.05})O_4]_2$ monoclinic	$Zr_2O[(P_{0.95}V_{0.05})O_4]_2$ monoclinic
Cat-24	$Zr_2O[(P_{1-x}V_x)O_4]_2$	XRPD: $Zr_2O(PO_4)_2$ orthorhombic	XRPD: $Zr_2O(PO_4)_2$ orthorhombic
Cat-25	"VNb_9O_{25}"	XRPD: *T*-Nb_2O_5 [51] broad reflections	XRPD: *T*-Nb_2O_5 [51] broad reflections
Cat-26	VNb_9O_{25}	XRPD: VNb_9O_{25}	XRPD: VNb_9O_{25}

Cat-27	"$(V_{0.5}P_{0.5})Nb_9O_{25}$"	XRPD: *T*-Nb_2O_5 [51] broad reflections; ^{31}P-MAS-NMR: δ_{iso} = -16.1 ppm	XRPD: *T*-Nb_2O_5 [51] broad reflections
Cat-28	$(V_{0.5}P_{0.5})Nb_9O_{25}$	XRPD: $(V_{0.5}P_{0.5})Nb_9O_{25}$; ^{31}P-MAS-NMR: δ_{iso} = -16.1 ppm	$(V_{0.5}P_{0.5})Nb_9O_{25}$
Cat-29	"$V^{IV}Nb^{V}(PO_4)_3$"	XRPD: amorphous	XRPD: amorphous

a) Compositions given in parentheses refer to overall chemical compositions only; in contrast formula without parentheses refer to a particular phase of given composition.

b) X-ray powder diffraction (XRPD; Guinier method and powder diffractometry; see section 2.2 and MAS-NMR spectroscopy using ^{31}P and ^{51}V nuclei have been used for characterization.

c) At testing conditions with higher amounts of *n*-butane in the gas mixture the starting material $(V^{IV}O)_2[B(OH)_4][PO_4]$ was stable

d) At testing conditions with higher amounts of *n*-butane in the gas mixture the starting material $V^{III}[B_2P_2O_7(OH)_5]$ was oxidized to $V^{III}V^{IV}{}_3O_3(PO_4)_3$ and BPO_4.

e) By ^{31}P- and ^{51}V-MAS-NMR spectroscopy pre-crystalline forms of β-$VOPO_4$ and $VOPO_4{\cdot}2H_2O/\alpha_I$-$VOPO_4$ (see text) are clearly indicated. As titanium-containing intermediate pre-crystalline $Ti_5O_4(PO_4)_4$ and, possibly, smaller amounts of $Ti(P_{1-x}V_x)_2O_7$ and/or $(VO)Ti_6(PO_4)_9$ are present. Due to similar range of chemical shift in ^{31}P-MAS-NMR [45,46] a clear distinction between the three phases in the amorphous material is impossible.

f) According to ^{31}P- and ^{51}V-MAS-NMR spectra the non-equilibrium mixture consists of pre-crystalline $Ti(P_{1-x}V_x)_2O_7$, β-$VOPO_4$ and $VOPO_4{\cdot}2H_2O/\alpha_I$-$VOPO_4$ (see text), and as additional titanium-containing phase pre-crystalline $Ti_5O_4(PO_4)_4$ and/or small amounts of $(VO)Ti_6(PO_4)_9$. Due to similar range of chemical shift in ^{31}P-MAS-NMR [45,46] a clear distinction between the three titanium-containing phases in the amorphous material is impossible.

g) According to ^{31}P- and ^{51}V-MAS-NMR spectra the amorphous V-rich $Ti(P_{1-x}V_x)_2O_7$ non-equilibrium mixture consists of pre-crystalline V_2O_5, β-$VOPO_4$ and small amounts of $VOPO_4{\cdot}2H_2O/\alpha_I$-$VOPO_4$. As titanium-containing phase pre-crystalline $Ti_5O_4(PO_4)_4$ was identified.

No.	Composition	ϑ (°C)	$X_{n\text{-butane}}$ (%)	S_{MA} (%)	S_{COx} (%) $^{CO2+CO}$
Cat-1 [a)]	"$Ag_2V^{IV,V}P_{1.6}O_{7+\delta}$"	430	24	13	80+7
Cat-2	$Ag(V^{IV}O)(V^{V}O)(PO_4)_2$	380	5	-	100+0
Cat-3	$(V^{IV}O)_2[B(OH)_4][PO_4]$	400	18	17	39+44
Cat-4	$V[B_2P_2O_7(OH)_5]$	450	63	5	23+72
Cat-5	$Fe_{0.5}V_{0.5}[B_2P_2O_7(OH)_5]$	450	16	6	38+56
Cat-6	$V^{III}{}_2[BP_3O_{12}]$	420	8	24	30+46
Cat-7	"$Fe(VO)(PO_4)_2$"	420	7	-	45+55
Cat-8	$Fe(VO)(PO_4)_2$	420	-	-	-
Cat-9	"$Fe_4[(P_{0.9}V_{0.1})_2O_7]_3$"	420	14	-	40+60
Cat-10	$Fe_4[(P_{0.9}V_{0.1})_2O_7]_3$	420	7	-	67+33
Cat-11	"$Fe_4[(P_{0.25}V_{0.75})_2O_7]_3$"	420	80	-	35+65
Cat-12	$Fe_4[(P_{0.25}V_{0.75})_2O_7]_3$	420	14	-	47+53
Cat-13	"$(VO)Ti_6(PO_4)_9$"	350	26	23	32+45
Cat-14	$(VO)Ti_6(PO_4)_9$	350	8	15	40+45
Cat-15	"$Ti(P_{0.8}V_{0.2})_2O_7$" P-rich	350	7	41	0+59
Cat-16	$Ti(P_{0.8}V_{0.2})_2O_7$ P-rich	350	15	14	35+51
Cat-17	"$Ti(P_{0.6}V_{0.4})_2O_7$" V-rich	350	59	13	35+52
Cat-18	$Ti(P_{0.6}V_{0.4})_2O_7$ V-rich	350	3	17	54+29
Cat-19	ZrV_2O_7	420	24	-	44+56
Cat-20	ZrV_2O_7	420	18	-	46+54
Cat-21	"$Zr(P_{0.5}V_{0.5})_2O_7$"	420	67	-	38+62
Cat-22	$Zr(P_{0.5}V_{0.5})_2O_7$	420	32	-	38+62
Cat-23	"$Zr_2O[(P_{0.95}V_{0.05})O_4]_2$"	420	53	-	43+57
Cat-24	$Zr_2O[(P_{0.95}V_{0.05})O_4]_2$	420	47	-	40+60
Cat-25	"VNb_9O_{25}"	420	99	-	100+0

Cat-26	VNb_9O_{25}	420	18	-	64+36
Cat-27	"$(V_{0.5}P_{0.5})Nb_9O_{25}$"	420	98	-	99+1
Cat-28	$(V_{0.5}P_{0.5})Nb_9O_{25}$	420	18	-	94+6
Cat-29	"$V^{IV}Nb^{V}(PO_4)_3$"	380	20	5	59+36

a) Compositions given in parentheses refer to overall chemical compositions only; in contrast formula without parentheses refer to a particular phase of given composition (seeTable 1).
b) Feed composition: *n*-butane / air / H_2O = 1.85 / 95.15 / 3
c) Specific butane conversion rate: {gas flow [$nL \cdot h^{-1}$] × $C_{n\text{-butane}}$ [vol-%] / 100 × $X_{n\text{-butane}}$[%] / 100} / / {22.4 [$nL \cdot mol^{-1}$] × m_{cat} [g] × S_{cat} [$m^2 \cdot g^{-1}$]}
d) Feed composition: *n*-butane / air / H_2O = 2.1 / 94.9 / 3

No.	compound	calculated Λ_o
Cat-1	$Ag_6(V^{IV}O)_2(PO_4)_2(P_2O_7)$	0.57
Cat-2	$Ag(V^{IV}O)(V^{V}O)(PO_4)_2$	0.52
Cat-3	$(V^{IV}O)_2[B(OH)_4][PO_4]$	0.50
Cat-4	$V^{III}[B_2P_2O_7(OH)_5]$	0.41
Cat-5	$Fe^{III}_{0.5}V^{III}_{0.5}[B_2P_2O_7(OH)_5]$	0.42 [a)]
Cat-6	$V^{III}_2[BP_3O_{12}]$	0.43 [a)]
Cat-8	$Fe(VO)(PO_4)_2$	0.49
Cat-10	$Fe_4[(P_{0.9}V_{0.1})_2O_7]_3$	0.51
Cat-12	$Fe_4[(P_{0.25}V_{0.75})_2O_7]_3$	0.65
Cat-14	$(VO)Ti_6(PO_4)_9$	0.49
Cat-16	$Ti(P_{0.8}V_{0.2})_2O_7$ (P-rich)	0.50
Cat-18	$Ti(P_{0.6}V_{0.4})_2O_7$ (V-rich)	0.55
Cat-20	ZrV_2O_7	0.70
Cat-22	$Zr(P_{0.5}V_{0.5})_2O_7$	0.57
Cat-23	$Zr_2O[(P_{0.95}V_{0.05})O_4]_2$	0.51
Cat-25	*T*-Nb_2O_5	0.61 [b)]
Cat-26	VNb_9O_{25}	0.61
Cat-28	$(V_{0.5}P_{0.5})Nb_9O_{25}$	0.60
Cat-29	$V^{IV}Nb^{V}(PO_4)_3$	0.45

a) $\Lambda_o(V_2O_3)$ used in the calculation has been chosen to be equal to $\Lambda_o(Cr_2O_3) = 0.70$.
b) $\Lambda_o(Nb_2O_5) = 0.70$ for Nb^{5+} in octahedral coordination.